Spring 5-4-2024

ELECTRICAL RESISTANCE TOMOGRAPHY MEASUREMENTS IN COLUMN FLOTATION OF PURE HYDROPHOBIC AND HYDROPHILIC SYSTEMS

Vimeipha Vilayphone

ELECTRICAL RESISTANCE TOMOGRAPHY MEASUREMENTS IN COLUMN FLOTATION OF PURE HYDROPHOBIC AND HYDROPHILIC SYSTEMS

by

Vimeipha Vilayphone

A thesis submitted in partial fulfillment of the
requirements for the degree of

Master of Science
Metallurgical and Mineral Processing Engineering

Montana Tech
2024

Abstract

Column flotation was phenomenologically investigated with Electrical Resistance Tomography (ERT) as an uninterrupted instrument to measure gas holdup. Two-phase tests were performed to use the measurements for examining gas dispersion. Results were found to duplicate the findings in a previous thesis. With confidence attained in experimental procedures, three-phase tests were then performed to compare gas holdup with hydrophobic and hydrophilic solids. Hydrophobic solids included talc as well as dolomite with dodecyl amine (DDA) collector. Hydrophilic solids included dolomite as well as talc with carboxymethyl cellulose (CMC) depressant. Variables throughout the research included frother concentration and sparger size. Results showed gas holdup for the hydrophobic systems was greater than that determined for hydrophilic systems. Furthermore, both systems showed the gas holdup increased with increasing frother concentration and increasing sparger size. When oleic acid (OA) was used as collector with dolomite for comparing to dolomite with DDA, the gas holdup increased further and was attributed to OA having frothing capability which is well-known. Gas holdup values were also used to explain gas dispersion and bubble size measurements emphasizing the importance of bubble-particle collisions and attachments for hydrophobic systems and the lack thereof in hydrophilic systems. Future studies on column flotation will benefit regarding computational modeling and use of collectors and collector blends on ores containing rare earth elements (REEs).

Dedication

This paper is dedicated to my family and metallurgical engineering colleagues for their endless inspiration and support.

Acknowledgements

I would like to express great thanks to Dr. Courtney Young and Dr. Richard LaDouceur for their considerable knowledge and experience in advising the research and development of this research. I would like to especially thank Dr. Mario Caccia for joining my thesis committee on last-minute notice and for applying his "external" knowledge to this flotation study. Thanks also go to Dr. Trenin Bayless and my colleague, Mitchell Harvey, for their direct assistance on the column flotation setup and sample acquisition. I also would like to acknowledge the helps of Dr. Peter Lucon and my other colleagues, Abdul Mamudu, Patrick “Jeff” Mensah, Ethan Mishler, Chance Green, Joe “Trip” Love, Layton Bahnmiller, David Rathgeber, and Padmore Amankwah for their time and contribution in obtaining the desired particle size distribution of the samples, photographs using the high-speed camera, and measurements of zeta potential/surface charge. Finally, I would like to thank DEVCOM Army Research for sponsoring this project.

Disclaimer

Research was sponsored by the DEVCOM Army Research Laboratory and was accomplished under Cooperative Agreement Number W911NF-22-2-0015. The views and conclusions contained in this document are those of the authors and should not be interpreted as representing the official policies, either expressed or implied, of the DEVCOM Army Research Laboratory or the U.S. Government. The U.S. Government is authorized to reproduce and distribute reprints for Government purposes notwithstanding any copyright notation herein.

List of Tables

Table 1: Two-factor Factorial Design 16
Table 2: Coefficient of Variance of Midpoint Test Gas Holdup (2.5-mm Sparger) 25
Table 3: Coefficient of Variance of Midpoint Test Gas Holdup (2.5-mm Sparger) 26
Table 4: Bubble Diameter Results Calculated by DFA 35
Table 5: Sparger Bubble Diameter Results at Plane 1 and Plane 2 (2.5-mm) 39
Table 6: Bubble Diameter Results in mm at Plane 1 and Plane 2 with increasing Solids Content (5.0-mm) 39

List of Figures

Figure 1: Column Flotation Schematic Diagram 4
Figure 2: Flow Regime in Column Flotation [10] 5
Figure 3: Process flow schematic for flotation showing typical phenomena [12] 8
Figure 4: Schematic Diagram and Actual Laboratory Apparatus 11
Figure 5: Internals of ERT Sensor (left); ERT Sensor at Montana Tech (middle); Unit Processor and Software (right) 13
Figure 6: Talc Crystallographic Structure [19] 14
Figure 7: Dolomite Crystal Structure [21] 14
Figure 8: Chemical Structure of Reagents (a) CMC [22], (b) DDA [23], and (c) OA [24] 14
Figure 9: Scheme of Experiment 16
Figure 10: Particle Size Distribution of Dolomite and Talc 19
Figure 11: BSE image of (a) Dolomite and (b) Talc 20
Figure 12: Chemical Composition of Dolomite and Talc 21
Figure 13: Zeta Potential Profile of Dolomite and Talc at Various pH 22
Figure 14: Gas Holdup Profile of Baseline Test (S = sparger size and F = frother concentration) 23
Figure 15: Minimum Dispersion of Hydrophilic (Dolomite) and Hydrophobic (Talc) Systems 24
Figure 16: Gas Holdups of Hydrophobic System (a) Dolomite, and (b) Talc and CMC, in a 2.5-mm Sparger Column Flotation Cell 27
Figure 17: Gas Holdups of Hydrophobic System (a) Dolomite, and (b) Talc and CMC, in a 5.0-mm Sparger Column Flotation Cell 28
Figure 18: Gas Holdups of Hydrophobic System (a) Talc, (b) Dolomite and DDA, and (c) Dolomite and Oleate, in a 2.5-mm Sparger Column Flotation Cell 30
Figure 19: Gas Holdups of Hydrophobic System (a) Talc, (b) Dolomite and DDA, and (c) Dolomite and Oleate, in a 5.0-mm Sparger Column Flotation Cell 31
Figure 20: Snapshots of Bubble Diameter using High-speed Camera (a) Overviews of Bubble with and without Frother Addition, and (b) Marks of Randomly Selected Bubbles 36
Figure 21: Bubble Diameter Results in mm of 2.5-mm (left) and 5.0-mm (right) Spargers 37

List of Appendices

Appendix A: ASTM Standard Test Methods for Determining Average Grain Size 50
Appendix B: 102 spots of randomly selected bubbles.....51

Glossary of Terms

BSE	Backscattered Electron
CMC	Carboxymethyl Cellulose
DDA	Dodecyl Amine
EDX	Energy Dispersive X-ray Spectroscopy
ERT	Electrical Resistance Tomography
OA	Oleic Acid
REE	Rare Earth Element
SEM	Scanning Electron Microscopy

Table of Contents

Abstract ii

Dedication iii

Acknowledgements iv

Disclaimer v

List of Tables vi

List of Figures vii

List of Appendices viii

Glossary of Terms ix

Introduction 1

Purpose 10

Methodology 11

Results and Discussion 19

- **Particle Size and Shape** 19
- **Gas Dispersion at Various Planes** 22
- **Gas Holdup** 25
- **Bubble Diameters** 33

Conclusions 42

Future Work and Recommendations 44

References 45

Appendices 50

Introduction

Flotation is a three-phase beneficiation technique that is used to separate valuable minerals from gangue based on differences in hydrophobicity [1]. In this regard, mineral particles are the solids, water is the liquid, and air generally serves as the gas albeit any gas can be used. Hydrophobicity is a chemical property of mineral surface that is either natural or induced using surfactants such as collector to promote and depressant to prevent [2]. In a flotation cell, chemistry, ore, and machine are involved to allow air bubbles and particles to interact. As the bubbles and particles collide and attach, they can be recovered from flotation system via three mechanisms including selective attachment of bubbles, entrainment in water that passes through to concentrate exit, and physical entrapment between particles and bubbles. Of these mechanisms, attachment is an ideal performance but real flotation plant may not always achieve this due to variations in chemical properties (e.g., material composition and hydrophobicity), physical properties (e.g., particle shape and size), and machine-driven variables (e.g., air rate and bubble size). Attachment is important as it is directly related to hydrophobicity of the minerals and represents the major portion of minerals recovered to the concentrate. On the other hand, entrainment and physical entrapment attributes separation efficiency and both gangue and valuable minerals can be recovered into concentrate via these mechanisms. Although drainage, which is the return of entrained and entrapped minerals into flotation pulp, occurred in froth phase which is above the pulp surface and overflows to send concentrate from system, various stage of flotation setup is still preferred to single flotation to achieve an economically acceptable concentrate product.

Surfaces of feed minerals can be categorized into nonpolar and polar types [2]. This is generally understood by employing zeta potential measurement to examine electrical charge on surface of materials which is predominantly influenced by pH. By nature, charges on surface of

materials can be both positive and negative and are balanced at a point of zero charge (PZC). The nonpolar type (positively and negatively balanced surface) possesses chemical structure of covalent molecules linked together by (weak) van der Waals force which makes the nonpolar minerals to be hydrophobic and resist reaction with water which is a polar solvent. On the opposite side, polar minerals (either positive or negative charge predominant) have strong covalent bonds and react instantly with water making them hydrophilic. In order to perform flotation efficiently, the flotation system must involve hydrophobicity which can be aided by adding collector or depressant to the pulp as already noted. Collectors are organic compounds that induce hydrophobicity to minerals by putting a hydrophobic film around the minerals surface. Due to collector possessing heteropolar molecular structure, they may interact with minerals via chemical adsorption "chemisorption" that adsorbs onto surface of minerals by forming chemical bonds and generate a monolayer. Collector may also interact with mineral surface via physical adsorption "physisorption" that adsorbs onto surface of minerals by coulombic attraction due to opposite charges between the collector and mineral surface. On the other hand, depressant is applied to gangue (semi-soluble salts) to prevent adsorption and flotation and interacts with gangue minerals similarly to collector interacting with valuable minerals.

With various designs available, regardless of complexity associated with flotation, upon flotation was invented more than 100 years ago, there have been a plethora of applications in the mineral industry. Technology has developed to the point where it can be used to process so-called uneconomical, low-grade, and complex ores. However, more attention is needed to improve it in terms of increased recovery and/or capacity [2]. With the initial development to treat sulfide minerals, flotation has evolved to also treat non-sulfide minerals such as soluble salts (e.g., halite), semi-soluble salts (e.g., dolomite), silicates (e.g., talc), oxides (e.g., hematite), and organic materials (e.g., coal) as well as non-mining commodities (e.g., paper

recycling, water treatment, and de-oiling systems) [3, 4, 5]. Flotation can be accomplished with a variety of unit operations including but not limited to mechanical agitation cells, columns, Jameson cells, and pipes. The latter is a new but developing technology. Research conducted for this thesis focused on column flotation and the application of Electrical Resistance Tomography (ERT) to conduct gas measurements to study responses of column flotation to process variables as discussed in Purpose and Methodology.

A schematic drawing of column flotation is displayed in Figure 1. Column flotation is considered a non-mechanical mixing type with bubble generated by a sparger at the bottom [6]. Because the sparger acts like a point source, the bubbles disperse axially as they rise. Feed enters the column as a slurry below the froth approximately third-way to half-way down the column. Particles in the feed sink in countercurrent flow to the rising bubbles. This allows the bubbles and particles to collide. Normally, valuable particles are hydrophobic minerals and thereby attach and float into the froth, forming a concentrate (i.e., con). Likewise, gangue particles are hydrophilic minerals and therefore do not attach and exit out the bottom as waste (i.e., tail). A water system may be installed in or above the froth to wet the froth. However, this “wash” water is also used as a positively biased flow to minimize and even prevent entrainment of hydrophilic particles.

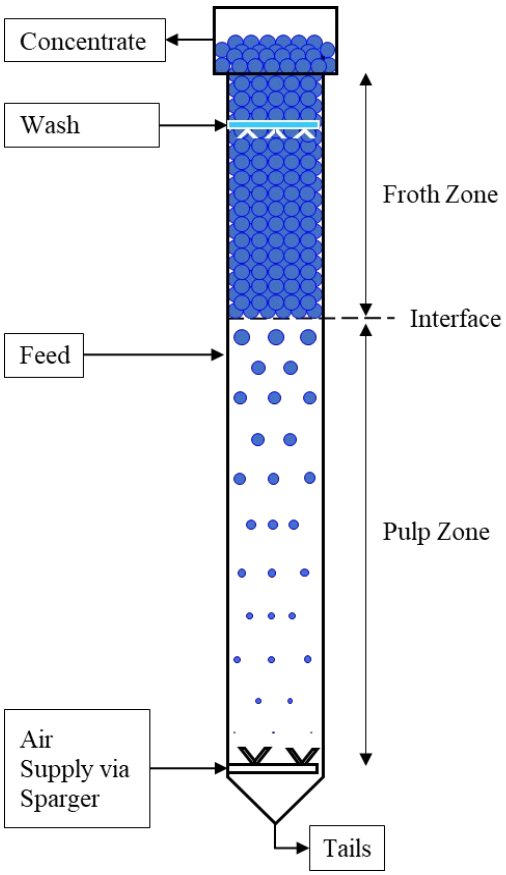

Figure 1: Column Flotation Schematic Diagram

For column flotation, the ratio of height to diameter is not fixed; however, this value is significantly higher compared to mechanical flotation [7]. While cross-sectional area affects throughput, the span of froth and pulp zones affect concentrate grade and recovery, respectively. Due to lack of mechanical mixing, column flotation has stronger quiescence and produces finer bubbles compared to mechanical agitation flotation. In this regard, column flotation can work on weakly hydrophobic particles and has become preferred in cleaning stages [7, 8]. However, its capacity is low in comparison and may not be appropriate for given systems.

In general, unit operations in flotation consist of two zones, one for the pulp with moderate bubble density and the other for the froth with significantly higher bubble density. However, more phenomena are identified later. The zones are separated from one another by an interface.

As shown in Figure 1, flotation columns are no different. The froth zone can contain up to 70% gas by volume, whereas the pulp zone can hold up to 20% [6, 9]. While this "gas holdup" is the key to understanding hydrodynamic conditions in the pulp zone, the interaction of froth and pulp zones impacts the overall performance of flotation column, emphasizing the importance of gas holdup [6]. Although the general design of column flotation promotes axial uniformity of bubbles, air flow can still vary between a desirable homogeneous or "bubbly" regime and an undesirable heterogeneous or turbulent regime referred to as "churn" (see Figure 2).

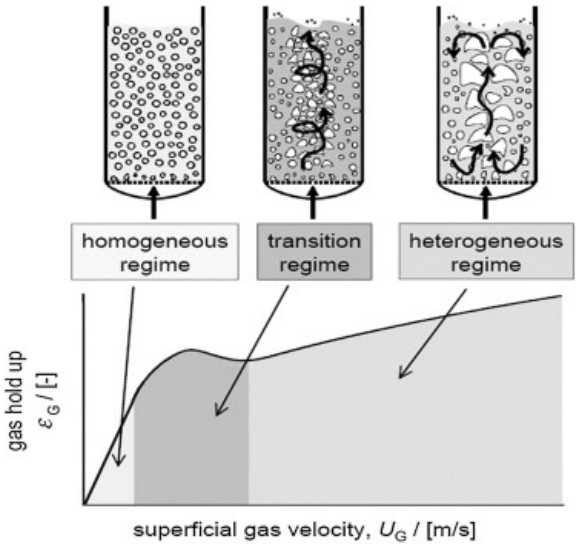

Figure 2: Flow Regime in Column Flotation [10]

Operating air flows are primarily influenced by two factors: superficial velocity and gas holdup. Superficial velocity is the ratio of air flow rate to column cross-sectional area. As just noted, gas holdup is the volume fraction of the column occupied by air and can vary with height in the column. A bubbly flow is developed when bubbles of the same size rise at the same flow rate leading to a linear relationship between superficial velocity and gas holdup as illustrated at low numbers by the plot in Figure 2. When the superficial velocity increases, gas flow becomes transitional such that the gas holdup changes nonlinearly and can even go through a maximum. Hence, in the transition regime, the gas holdup may increase or decrease slightly. If the superficial velocity continues to increase further, churn turbulent flow will occur. In this

zone, large bubbles rise quickly, driving smaller bubbles away from the axial direction. This can push the bubbles downward, resulting in an unstable gas holdup. The air flow rate is therefore limited by the response of flow behavior being observed.

A review on publications of column flotation modeling was conducted and reported that modeling tended to focus on recovery prediction and process dynamic behavior and that analyses were either partially or completely empirical [9]. Consequently, various approaches were taken; hence, models based on recovery prediction were developed with different strategies. Examples include but are not limited to using [9]:

- principles of fluid flow and particle buoyancy to explain mass balance; and first principles to explain bubble-particle attachment;
- air and water mass balance to approximate five compartments and then using distributed volume mixers-in-series instead of axially dispersed plug flow to increase the model efficiency;
- population balance technique to investigate various zones including aeration zone (perfectly mixed), lower and upper collection zone, feed zone, interface, and froth zone (with and without wash water);
- hydrodynamic principles with the emphasis on sparger and wash water system;
- first principles and neutral networks as a hybrid model to estimate the recovery of negative bias column flotation; and
- empirical regression models for assessing kinetics including stabilization following disturbances.

On the other hand, various models based on process dynamic behavior were also developed. These included using [9]:

- empirical techniques (e.g., fuzzy models, transfer function, and state-space applications) to predict variable behavior (e.g., grade, froth depth and gas holdup);
- experimental testing to determine connections between variables (e.g., bubble surface area flux, froth depth, gas holdup, and wash water flow rate) and metallurgical performance (e.g., grade and recovery);
- regression analyses of the effects of those and other variables (e.g., metallurgical performance, entrainment, drainage, and floatability) for flotation behavior prediction.

Empirical modeling can be used for low-cost projects such as designing a small-scale mining project or scoping the geo-metallurgical test work where the corrections to under-designing are small and timely [11]. However, due to drawbacks of empirical modeling that reflect unmatched experiences and benchmarks associated with laboratory practices or standards, using empirical models to design a flotation circuit for large mining projects involve risks that likely cause increased capital costs due to under-designing. As an alternative, phenomenological modeling approaches mathematically simulate the underlying mass transfer data obtained from test work to predict plant performance. With more understanding and accessibility of phenomenological models, it is increasingly relied on by industry.

Figure 3 shows flotation phenomena which can be summarized into three basic steps including bubble-particle collision, bubble-particle attachment, and bubble-particle detachment [12]. The variables that influence these phenomena consist of hydrodynamic parameters (bubble generation, air flow rate, and flow regime), chemical parameters (mineral dissolution, reagent, dosage, and chemistry for both surfaces and solutions) and mechanical parameters (particle size distribution, particle-bubble interaction, and froth drainage).

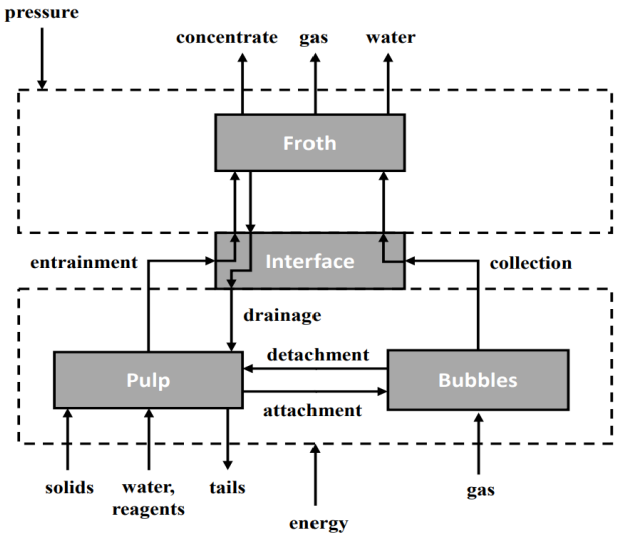

Figure 3: Process flow schematic for flotation showing typical phenomena [12]

ERT was originally developed as a technique to measure electrical resistivity for environmental management [13]. The measurement can be conducted on a linear and non-linear geometry (e.g., flat surface and vertical electrical sounding), in a borehole, or on the surface of water. The electrical resistivity data is used to generate electrical images of two dimensions (e.g., cross-sectional area) or three dimensions (e.g., pattern of belowground). With the ability to measure data without impacting the environment to generate spatial distribution of subsurface, ERT has been incorporated into the process industry to examine and characterize two-dimensional patterns in real time by conductivity imaging inside an object [14]. The principle behind obtaining gas holdup by ERT is via the measurement of conductivity variation as the system runs and changes overtime [15]. Then, by using Maxwell's equation, the gas holdup values can be derived from conductivity variation (see Methodology). It has been shown that ERT can be used to study gas behavior in both columns and mechanical agitation cells to examine the effects of frother, solids content, hydrodynamic behavior, as well as bubble size and loading [15, 16, 17]. For these reasons, ERT is known to be well-suited to phenomenologically investigate gas behavior during flotation. In this thesis, ERT is specifically

used to study the effects of hydrophobic and hydrophilic systems on gas holdup, gas dispersion, and bubble size as a function of frother concentration, percent solids and sparger size.

Purpose

Under the umbrella of column flotation, this thesis continues the research completed by a previous researcher [15] regarding the determination of variables related to gas holdup thereby drawing upon successful results obtained with a mechanical agitation cell [11, 12]. This will be accomplished using ERT to measure and study gas holdup as a function of purely hydrophobic and hydrophilic solids as well as frother concentration and sparger size. Results are expected to correlate to gas dispersion and bubble size. This understanding will serve as a foundation for furthering the development of phenomenological, compartmental model for flotation columns and should be applicable to mechanical agitation cells as well.

Methodology

Eriez supplied a flotation column that was 2.0-m high and had a 10.0-m inner diameter. It came with two interchangeable, 2.5 and 5.0-mm, cavitation-tube spargers. Upon arrival, the column was equipped with two ERT units and one unit processor from Industrial Tomography Systems (ITS). The combined apparatus is illustrated in Figure 4.

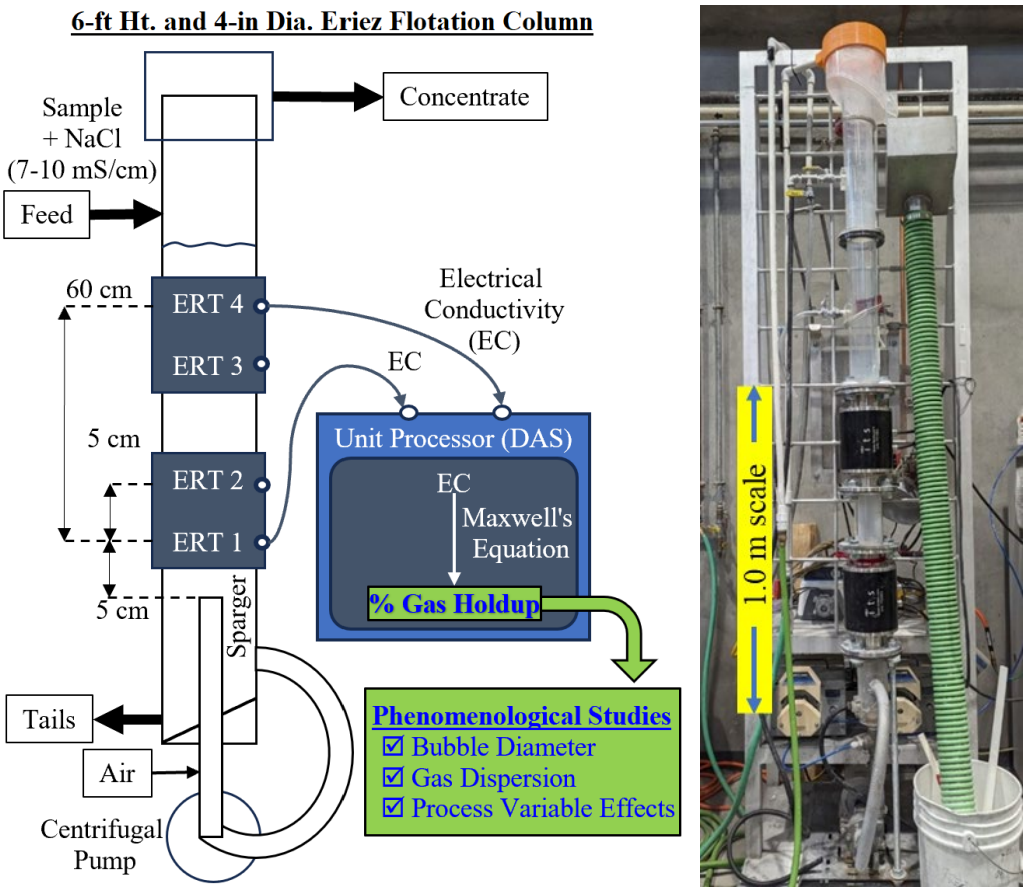

Figure 4: Schematic Diagram and Actual Laboratory Apparatus

In Figure 4, the ERT units measured conductivity at four different heights of the column, denoting plane 1 (the lowest position), plane 2, plane 3 and plane 4 (the highest position). A single ERT unit has two conductivity sensors that are 5 mm apart and can be located at any height along the column. Since gas behavior was interested within 70 cm above the sparger, this research stacked two ERT with a free space 10 cm between. Figure 5 shows the internal and external appearances of ERT units at the Metallurgical & Materials Engineering

Laboratories at Montana Tech. Each ERT unit is equipped inside with 16 conductivity probes installed with equal spacing among them at both upper and lower planes. When operating, the measured electrical current is connected to the unit processor to generate a two-dimensional image of the spatial distribution inside the flotation vessel. Because the electrical conductivity of air (gas phase) is negligibly small, air is considered as non-conductive phase. On the other hand, prior to starting the measurement, all test sample slurries are made to be conductive phase by mixing the samples with sodium chloride (NaCl) to obtain 7-10 mS/cm, sufficient to measure changes of volumetric fraction while posting negligible or no impact on flotation tests. Conductivity measured by ERT was analyzed by the ITS unit processor and p2k software which employed Maxwell's equation to convert the value to gas holdup. By using Maxwell's equation for spheres that relates conductivity to volumetric fraction (gas holdup), as shown in Equation 1, the conductivity of a gas holdup (k_m) can be identified as a function of conductivity between the conductive phase (k_c) and gas holdup (ε), as shown in Equation 2 [18]. The conductivity of gas holdup and conductive sample slurry are then used to find to value of gas holdup.

$$k_m = \left(\frac{1-\varepsilon}{1+0.5\varepsilon}\right) * k_c$$

Equation 1: Conductivity of Volumetric Fraction (Gas Holdup)

$$\varepsilon = \frac{1-\frac{k_m}{k_c}}{1+0.5*\frac{k_m}{k_c}}$$

Equation 2: Gas Holdup

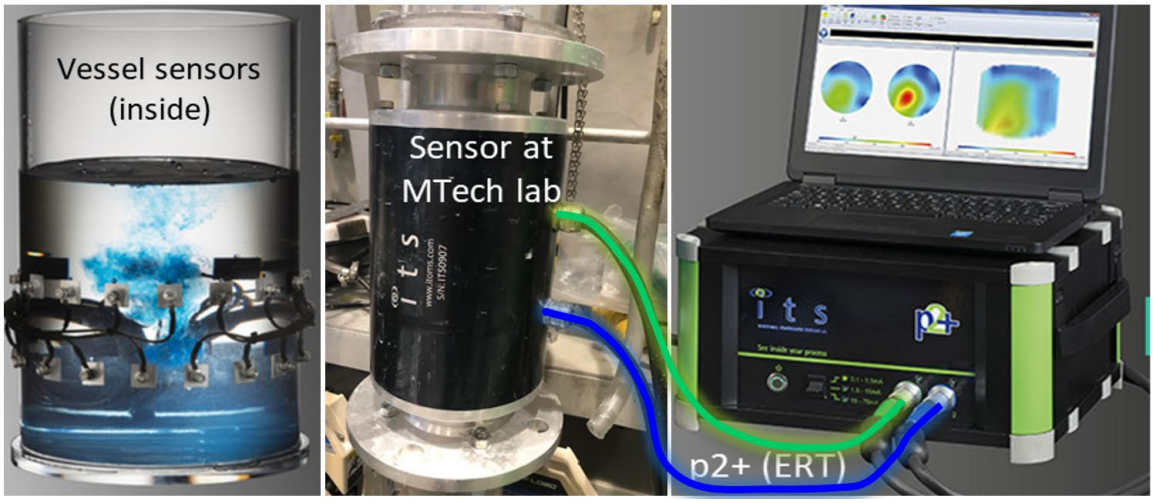

Figure 5: Internals of ERT Sensor (left); ERT Sensor at Montana Tech (middle); Unit Processor and Software (right)

Before running any experiment, the appropriate sparger was installed. Three different setups were used to conduct baseline tests, purely hydrophilic solids, and purely hydrophobic solids. Baseline tests were two-phased consisting of only air and water. Hydrophilic or hydrophobic solids were then added to make the tests three-phased.

Figure 6, Figure 7, and Figure 8 shows crystal and chemical structures of solid samples (dolomite and talc) and reagents Carboxy Methyl Cellulose (CMC), Dodecyl Amine (DDA), and Oleic Acid. Hydrophilic tests involved purely hydrophilic dolomite or naturally hydrophobic talc that was made hydrophilic with CMC depressant. The crystal structure of talc is composed of basal faces (hydrophobic) and edges (hydrophilic) [19]; therefore, when in fine size, basal faces can account for up to 90% of total surface area making talc highly hydrophobic. On the other hand, CMC can depress the floatability of talc by chemically adsorbing as a monolayer on the basal plane to create hydrogen and hydrophobic bonds that make the talc hydrophilic [20]. On the other hand, hydrophobic tests consisted of purely hydrophobic talc or dolomite made hydrophobic with Dodecyl Amine (DDA) collector. Unlike talc, all faces of dolomite crystal structure carry hydrophilic properties [21]. In this regard,

dolomite must be made hydrophobic through adsorption of collectors such as DDA and OA, usually physisorption due to interaction of opposite charges between the collector and dolomite surface [22]. However, these collectors can also chemically bond with dolomite in which as chemisorption occurs. In both cases, an initially formed monolayer can shift to bilayer and multilayer as a result of surface precipitation, if high collector concentrations are used [23]. Hydrophobic dolomite experiments were therefore conducted with DDA and OA. All experiments were completed using a Methyl Isobutyl Carbinol (MIBC) frother supplied by Syensqo (formerly Cytec).

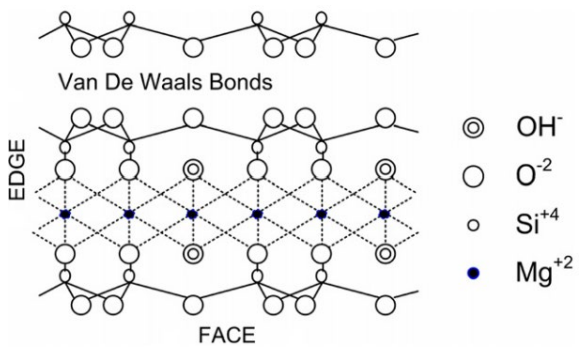

Figure 6: Talc Crystallographic Structure [19]

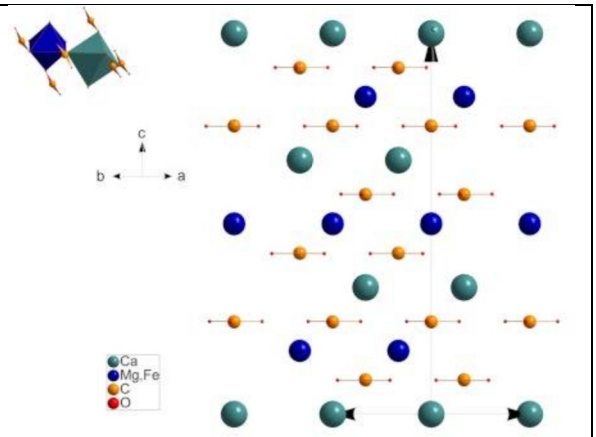

Figure 7: Dolomite Crystal Structure [21]

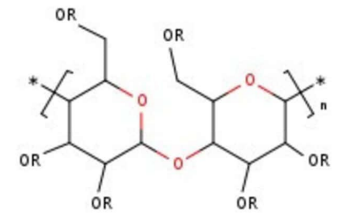

(a) CMC

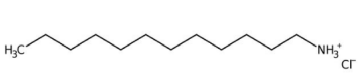

(b) DDA

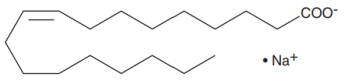

(c) OA

Figure 8: Chemical Structure of Reagents (a) CMC [22], (b) DDA [23], and (c) OA [24]

Tap water was used as the liquid phase component for all samples. With tap water being fresh and having conductivity less than 0.1 mS/cm, negligible to no reaction with solids and reagent

samples is expected. The solid samples (dolomite and talc) were sourced from Spring Hill Campground in Deer Lodge and Barrett's Minerals Inc in Dillon, Montana, respectively. The minerals had different theoretical densities, 2.70 g/cm^3 for talc and 2.82 g/ cm^3 for dolomite. Both samplers were comminuted using laboratory jaw crusher and rod mill to reduce the particle size to 80% passing at 75 microns. Upon grinding both samples using a jaw crusher to bring particle size down to less than 10.0 cm, 5.0-kg of dolomite was dry ground in a rod mill for 75 min. As talc is a softer material, 12.0-kg of talc was dry grinded by a rod mill for 65 min. The comminuted product of each solid were split using a rotary sample splitter to representatively divide the sample into smaller portions. A portion of split samples underwent size analysis using wet sieving to check and ensure similar particle size profiles of dolomite and talc. However, it is understood that particle shape will somewhat vary with naturally hydrophobic talc being trioctahedral and layered and naturally hydrophilic dolomite being trigonal with rhombohedral habit. Another portion was analyzed by Scanning Electron Microscopy-Energy Dispersive X-ray Spectroscopy (SEM-EDX) with Backscattered Electron (BSE) imaging of the elemental composition and particle shape as well as zeta potential measurements with Malvern Zeta sizer for surface charge quantification. Both fine dolomite and talc samples were coated with gold and taped with carbon to the sample stubs, the selection of sample points to zap for taking BSE images and analyzing elemental composition was ensured to be larger than 5 um and flat surface to comply with volume of interaction and avoid population bias. Additionally, the

The rest of solids were split into 1.75-kg samples as needed for each column flotation test. Experiments were conducted as two-factorial design of experiment (DOE) studies. The main factors were weight % solids (2, 5, and 8%) and frother concentration (10, 20 and 30 ppm) with gas holdup being the only response (see Table 1). The design resulted in seven experiments for each test scenario; single test for low-low (2% and 10 ppm), low-high (2% and 30 ppm), high-

low (8% and 10 ppm) and high-high (8% and 30 ppm) and triple tests for midpoint (5% and 20 ppm). All test scenarios required to investigate gas holdup are shown in Figure 5.

Table 1: Two-factor Factorial Design

		Solids by weight (%)		
		2	5	8
Frother concentration (ppm)	10	1 test		1 test
	20		3 tests	
	30	1 test		1 test

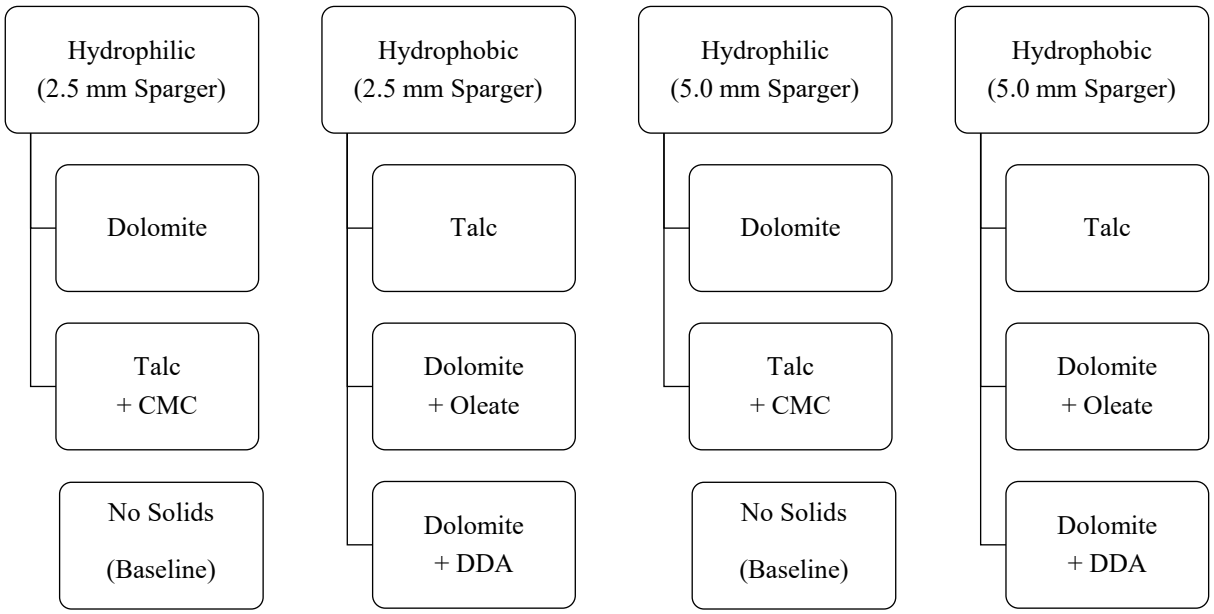

Figure 9: Scheme of Experiment

Each sample was prepared by adjusting the amount of water to achieve a desired solid content and reported as % solids by weight. Subsequently, the solid and water components were mixed to obtain a total volume of 5.0 l before mixing with NaCl to bring the solution conductivity to 7-10 mS/cm. The depressant CMC was mixed with talc; and the collectors (DDA and OA) were mixed dolomite at reagent to solid ratio of 1:2000 (i.e., 1 mg of CMC for 2.0 g of talc). The reagents were first dissolved in water before mixing with the sample slurry. For CMC and DDA, tests did not require pH adjustment; however, for OA, HCl was added to control the pH at 6. Conditioning times were typically 10 min for all tests before flotation commenced.

Spargers were switched as needed; however, this required the column to be disassembled and reassembled. In addition, four tests were conducted with only the 2.5-mm sparger to verify gas dispersion from the previous research by duplicating the results.

The steps to set up and measure gas holdup of each test are elaborated below:

1. To start a column flotation test, it is important to note that level of pulp surface inside the column is above the ERT probes prior to turning on the ERT and ITS unit processor.
2. Firstly, the sparger must be turned on and adjusted to the desired speed using tachometer (General Radiation Company, Strobotac Type 1531) to measure the RPM.
3. Then, feed pump is turned on to start feeding sample into the column; prior to drawing sample slurry, frother of desired concentration is firstly injected using a micropipette into the suction of feed pipe that is held by hand in an upright position to prevent back flow of the injected frother.
4. Once all frother is dosed, maintain the suction of feed pipe in an upright position and submerge it into the sample to draw the slurry and ensure no escape of frother into the sample bucket; let the sample transfer into the column completely then turn off the feed pump. In this regard, sample and frother are mixed in both feed pipe and column.
5. When the sample and frother are inside the column, ERT and ITS unit processor can be turned on for conductivity, amperage, and voltage calibrations.
6. Upon calibration, air can be supplied at required flow rate of 1.5 l/min for the 2.5-mm sparge and 2.0 l/min for the 5.0-mm sparger.
7. It is critical to note that air supply pressure and sparger speed must be reset at 70 psi and 1480 RPM for all tests, respectively, because the system does not return automatically to them.
8. A test is stopped after collecting sufficient data or upon reaching steady-state. At this point, the air supply, ERT, and ITS processor are shut off. The sparger can be left

running to flush and clean residuals inside the pump chamber, until clear water is observed.

9. Repeat step 2 to 8 until all tests are complete.

Results and Discussion

Particle Size and Shape

Upon comminuting both dolomite and talc samples, a representative portion of each was obtained using a rotary splitter. The split samples underwent wet sieving analysis to obtain particle size distribution results shown in Figure 6. Both solid samples were processed to have similar particle size profiles that satisfied the 80% passing at 75 μm.

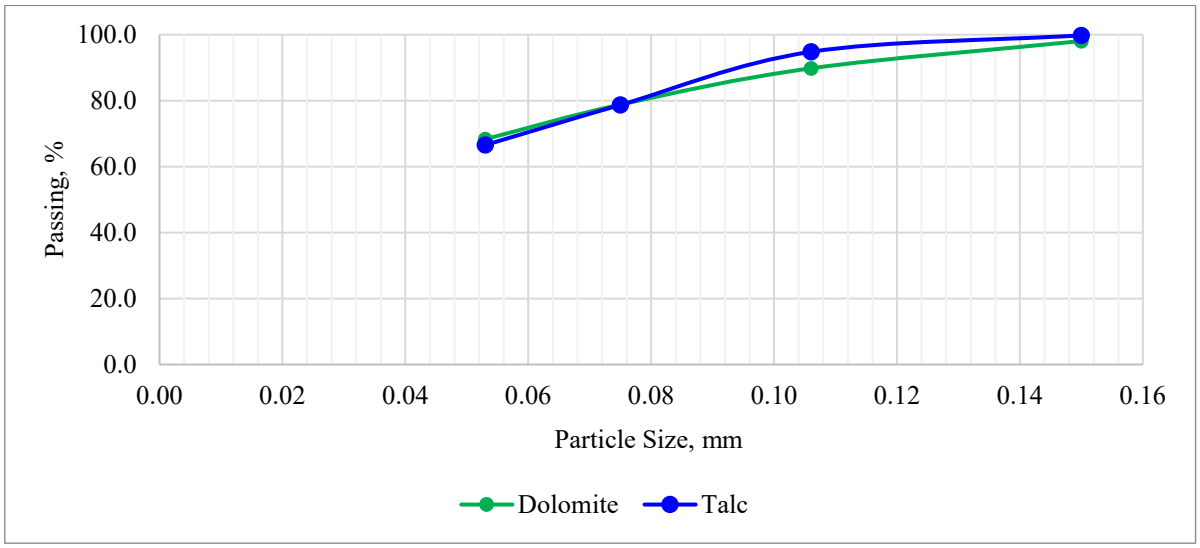

Figure 10: Particle Size Distribution of Dolomite and Talc

Figure 7 displayed BSE images of dolomite and talc fine particles using SEM. The images showed the distinctive size, shape, and surface between the two solids. The dolomite particles possessed sharp-edged granular structure indicative of breakage along cleavage planes, whereas talc particles possessed round-edged granular patterns indicative of a soft material. It is surprising to note that the talc did not exhibit platy particles and showed high basal surface which is hydrophobic [25]. Furthermore, it is noted that dolomite particles may be angular for smaller fines and cubic or rhombohedral for larger fines.

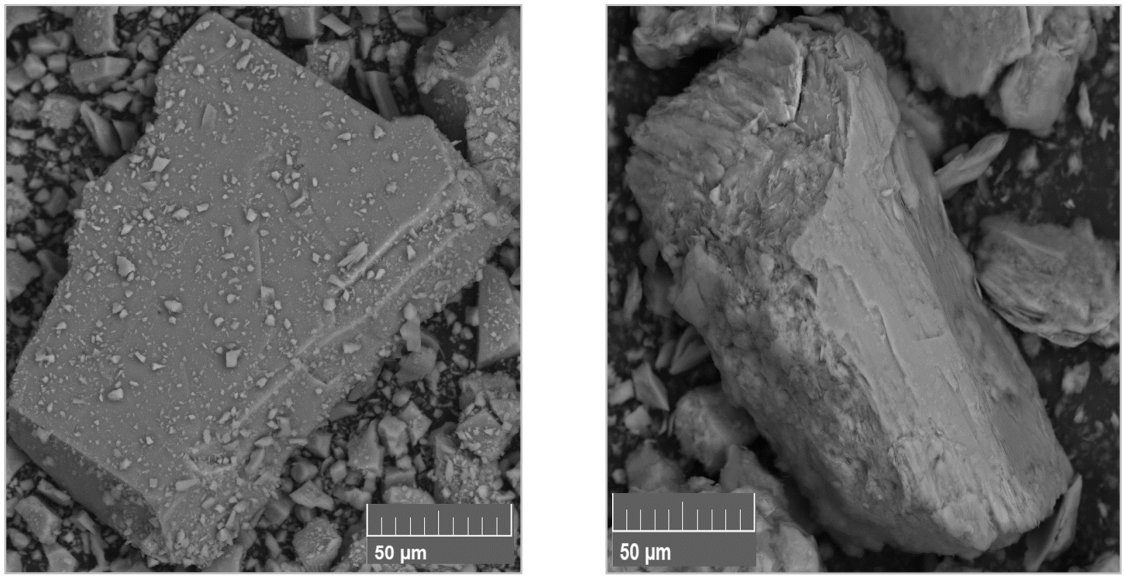

(a) Dolomite (b) Talc

Figure 11: BSE image of (a) Dolomite and (b) Talc

After obtaining BSE images, EDX analyses were conducted to obtain the chemical composition of both samples. Various spots on each sample were selected for elemental analysis. The concentrations of the key elements of dolomite ($CaMg(CO_3)_2$) namely carbon, calcium, magnesium and oxygen as well as that of talc ($Mg_3Si_4O_{10}(OH)_2$) namely magnesium, silica, oxygen and hydrogen were averaged and compared against literature denoted by dolomite (Lit) and talc (Lit) in Figure 8, respectively [26]. The results suggested that the samples used were pure dolomite and talc.

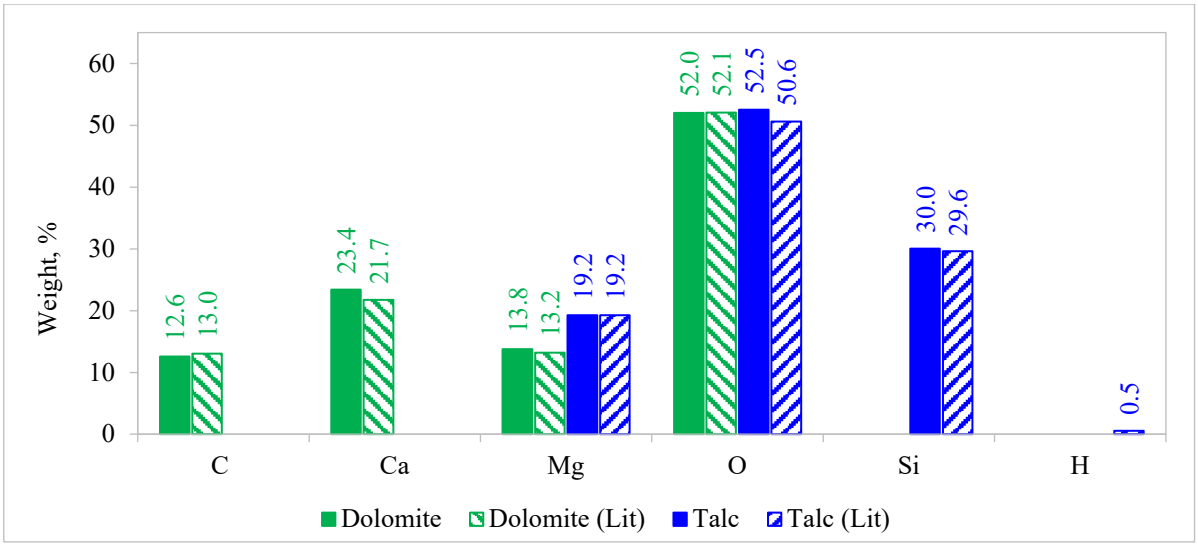

Figure 12: Chemical Composition of Dolomite and Talc

Figure 9 depicts profiles of dolomite and talc zeta potential from pH 2 to 12. The surface charge of dolomite was all positive and increased with pH while that of talc changed to negative polarity in between pH 3.0 and 3.5. Zeta potential measurements of both dolomite and talc were compared against literatures. While a few sources showed isoelectric point of dolomite to be between 6 and 8 [27, 28], a few more recent papers observed dolomite to be a positively charged surface at all pH values [29, 30]. On the other hand, talc zeta potential measurement similarly reflected findings in the literature confirming surface charge of talc to be negatively charged with isoelectric point close to the range provided in literature, pH 2 and 3 [25]. This indicated hydrophilic property of dolomite and highly hydrophobic property of talc. For a bubble-particle aggregate to form upon collision in flotation, the wetting film that was created when liquid spread across surface of solids must be ruptured first then form three-phase contact (attachment of solid, liquid and air) [31]. The stability of wetting film and kinetics of three-phase contact were highly dependent on surface hydrophobicity and surface electric charge [32]. For the highly hydrophobic cases, the effect of surface roughness is more critical than surface charge implying a strong correlational relationship between surface roughness and bubble-particle attachment [33].

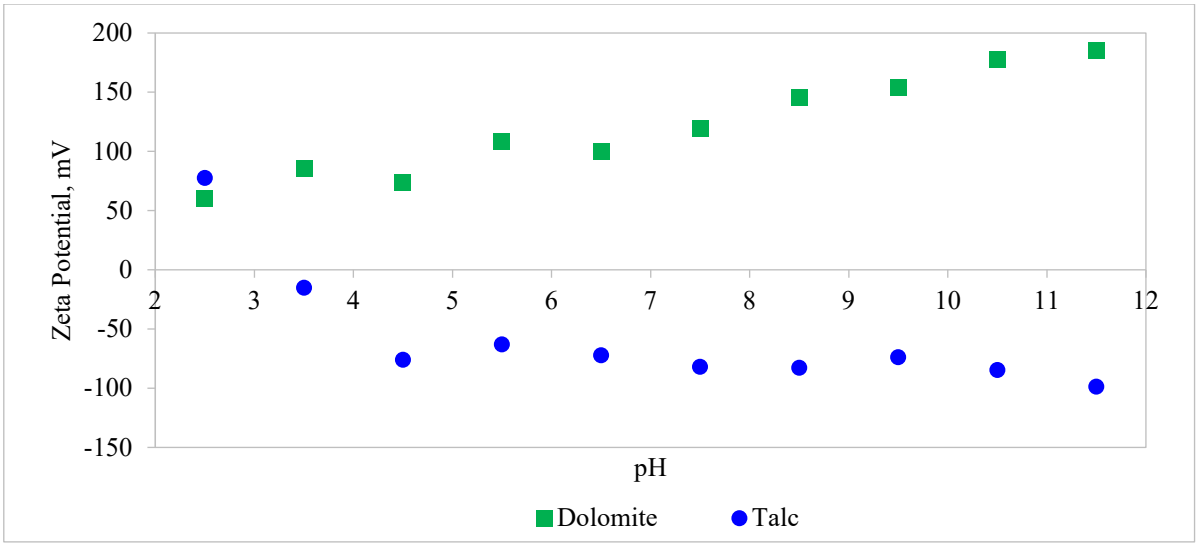

Figure 13: Zeta Potential Profile of Dolomite and Talc at Various pH

Gas Dispersion at Various Planes

The gas holdup profiles of baseline tests using both spargers (S = 2.5 mm and S = 5.0 mm) at frother concentration lower limit (F = 10 ppm) and upper limit (F = 30 ppm) are graphically summarized in Figure 10. All tests showed the same trend where Plane 1 gas holdup value being the lowest and changes in gas holdup at Plane 2, Plane 3 and Plane 4 were negligibly slight, excepting for the case of S = 5.0 mm and F = 30 mm that the gas holdup gradually decreased in Plane 3 and 4 upon reaching the highest value at Plane 2. This could mean the larger sparger and higher frother concentration easily shifted flow behavior from an ideal bubbly to a less bubbly/transitional flow regime. However, the unchanging gas holdup after Plane 2 showed a complete gas dispersion being reached by Plane 2 which was only 5 cm above Plane 1 and about 10 cm above the sparger, the same extent as the column diameter. Similar findings were also reported in the literature [15].

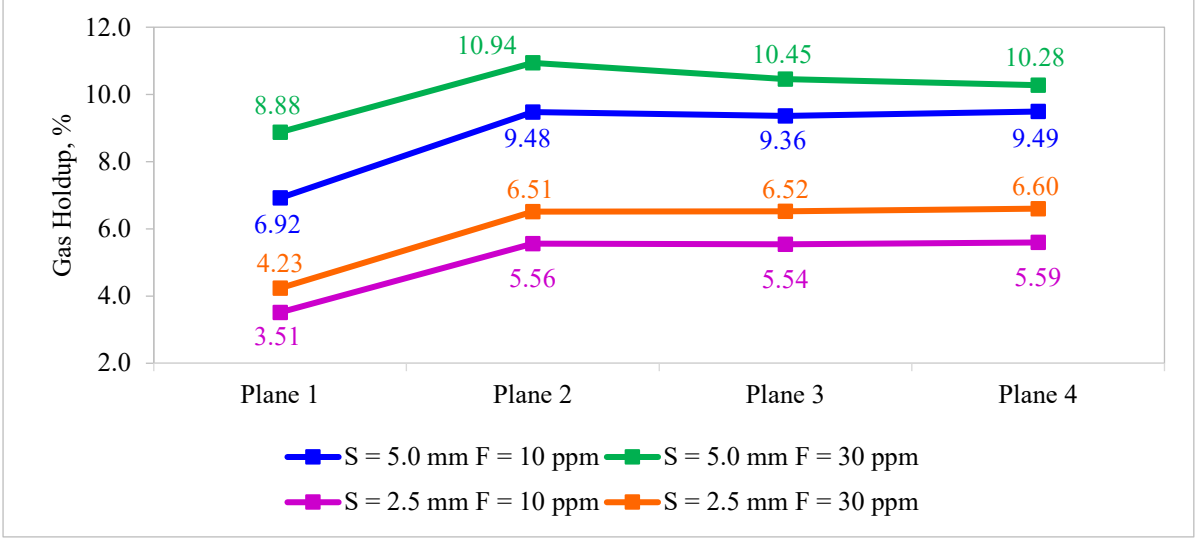

Figure 14: Gas Holdup Profile of Baseline Test (S = sparger size and F = frother concentration)

The gas dispersion behaviour of hydrophilic and hydrophobic systems of the extreme case (2% solid at 0 ppm and10 ppm frother concentrations) are portrayed in Figure 11. The natural behaviours of hydrophilic and hydrophobic particles in column cells were reflected by the no frother concentration scenario (0 ppm). The hydrophilic system reached fully dispersed gas immediately by Plane 2 while hydrophobic system required a longer time to reach fully dispersed gas in Plane 3. However, in the presence of minimum concentration (critical coalescence concentration of MIBC being 10 ppm [34]), gas in both systems became fully dispersed by Plane 2, reflecting on the findings as in the literature [15]. For the case of talc, gas holdup seemed to increase slightly at a higher plane (4.32, 4.49 and 4.60%) which could be due to higher collection of solids onto bubble as the bubble rose upward. In this section, only the trends of gas holdup at each plane were investigated for comparing gas dispersion development in hydrophilic and hydrophobic system in the column. A comparison among magnitudes of gas holdups between each system are discussed in Bubble Diameter.

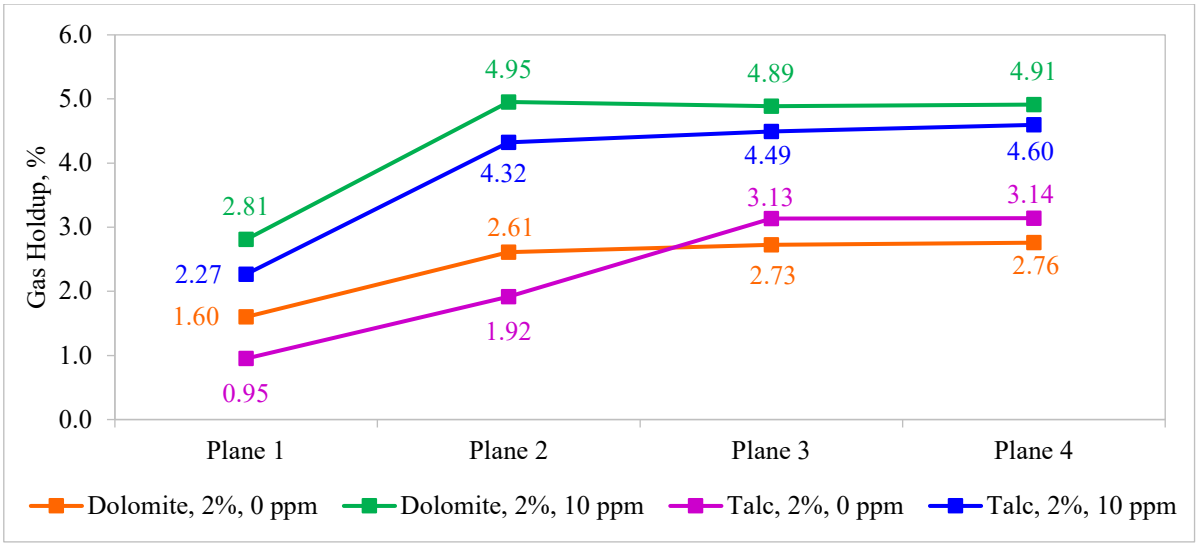

Figure 15: Minimum Dispersion of Hydrophilic (Dolomite) and Hydrophobic (Talc) Systems

Gas Holdup

Gas holdup profiles of each test scenario were summarized by averaging values measured at Plane 1 and Plane 2, instead of using only the fully dispersed plane data. This was because the gas holdup values measured at plane 2 of some tests were almost identical leading to insignificant interpretation of the data. In addition, by averaging gas holdup values at both planes, three-phase phenomena at the dispersing and fully dispersed plane were included in the investigation altogether. An analysis and discussion of gas dispersion between hydrophilic and hydrophobic systems as well as their impacts on bubble diameter are also made following the gas holdup analysis between the two systems.

The calculation of mean value between Plane 1 and 2, standard deviation, and coefficient of variance (CV) of each test was conducted to analyze the reproducibility of data in Table 2 and Table 3. For the 2.5-mm sparger (Table 2), all tests were in the acceptable range of CV (lower than 5.0%). The hydrophilic tests, dolomite and talc mixing with CMC, contained CV of 1.15 and 2.40% while hydrophobic tests including talc, dolomite mixing with DDA, and dolomite mixing with Oleate were represented by CV of 2.61, 1.11 and 0.33% respectively, indicating reproducibility of data.

Table 2: Coefficient of Variance of Midpoint Test Gas Holdup (2.5-mm Sparger)

Gas Holdup of Midpoint Tests (2.5-mm Sparger)					
	Dolomite	Talc + CMC	Talc	Dolomite + DDA	Dolomite + Oleate
Plane 1 - T3	2.283	2.225	1.741	2.193	3.339
Plane 1 - T4	2.340	1.925	1.83	2.469	2.826
Plane 1 - T5	2.381	2.195	1.807	1.971	2.928
Plane 2 - T3	6.538	6.128	7.177	7.697	9.07
Plane 2 - T4	6.685	6.787	7.319	7.376	9.506
Plane 2 - T5	6.564	6.514	7.589	7.712	9.419
Plane 1-2 Mean	4.465	4.296	4.577	4.903	6.181
Plane 1-2 Std dev.	0.051	0.103	0.119	0.054	0.02
Plane 1-2 CV	1.15%	2.40%	2.61%	1.11%	0.33%

On the other hand, all CV values of the hydrophobic tests with the larger sparger (5.0-mm) were slightly higher than those of the hydrophobic tests (Table 3). The hydrophilic tests showed CV of 3.78% for pure dolomite and 5.02% for talc mixing with CMC. The hydrophobic tests showed CV of 3.68% for pure talc, 2.68% for dolomite mixing with DDA, and 2.55% for Dolomite mixing with Oleate. The higher variance associated with larger sparger could be due to the likelihood the larger sparger can easily induce a turbulent flow regime.

Table 3: Coefficient of Variance of Midpoint Test Gas Holdup (2.5-mm Sparger)

Gas Holdup of midpoint tests (5.0-mm Sparger)					
	Dolomite	Talc + CMC	Talc	Dolomite + DDA	Dolomite + Oleate
Plane 1 - T3	9.169	8.548	8.478	9.500	9.637
Plane 1 - T4	8.806	8.243	8.352	9.442	9.897
Plane 1 - T5	9.320	7.568	8.948	8.757	9.306
Plane 2 - T3	10.370	8.918	8.517	13.588	11.865
Plane 2 - T4	10.687	10.566	8.559	13.237	11.874
Plane 2 - T5	11.503	9.549	9.107	13.140	11.418
Plane 1-2 Mean	9.976	8.898	8.660	11.277	10.666
Plane 1-2 Std dev.	0.377	0.447	0.319	0.303	0.272
Plane 1-2 CV	3.78%	5.02%	3.68%	2.68%	2.55%

Figure 12 and Figure 13 displays gas holdup results of a hydrophilic system in a 2.5 and 5.0-mm sparger respectively. From both figures, the gas holdup of pure dolomite decreased with weight percent solids as well as frother concentrations for both sparger sizes. In addition, with CMC having the ability to depressant talc [35], the same relationship was observed in the hydrophobic talc made hydrophilic by CMC. The presence of hydrophilic materials decreasing gas holdup was also observed with solid concentrations as well as particle size by literature [36]. The main reason driving this phenomenon could be because of collision and coalescence. Upon bubble colliding with particles, instead of attaching and collecting the particles upward, the collision may be immediately followed by detachment. Another reason could be the wetting film that was created upon liquid coating surface of the particles repelled bubbles after bubble-

particle collision creating a momentum that diverted the bubbles to coalesce into a larger size bubble allowing it to rise at a faster speed due to higher buoyancy force. The higher solid content as well as higher frother concentration may further exacerbate the concept due to more presence of hydrophilic solids and bubbles.

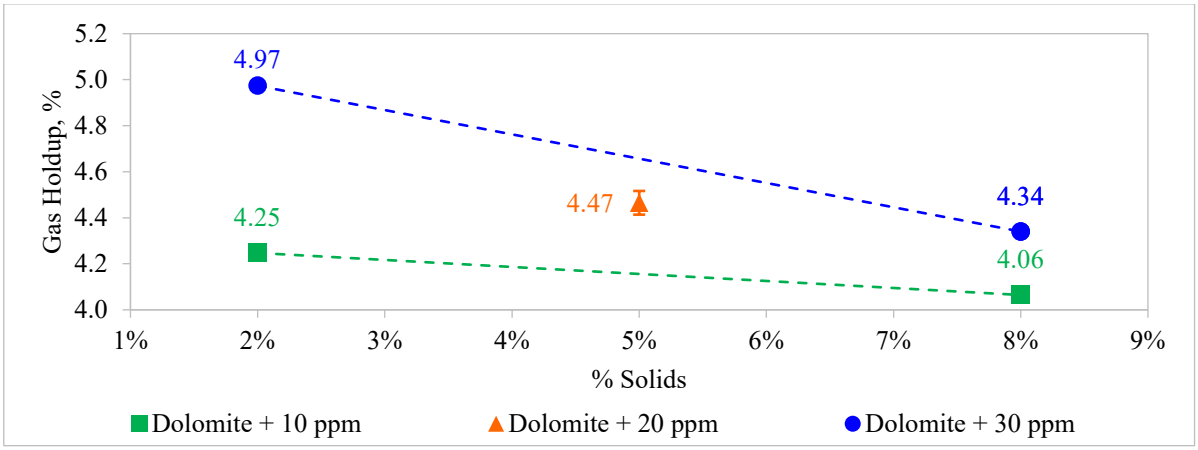

(a) Dolomite with 2.5 mm Sparger

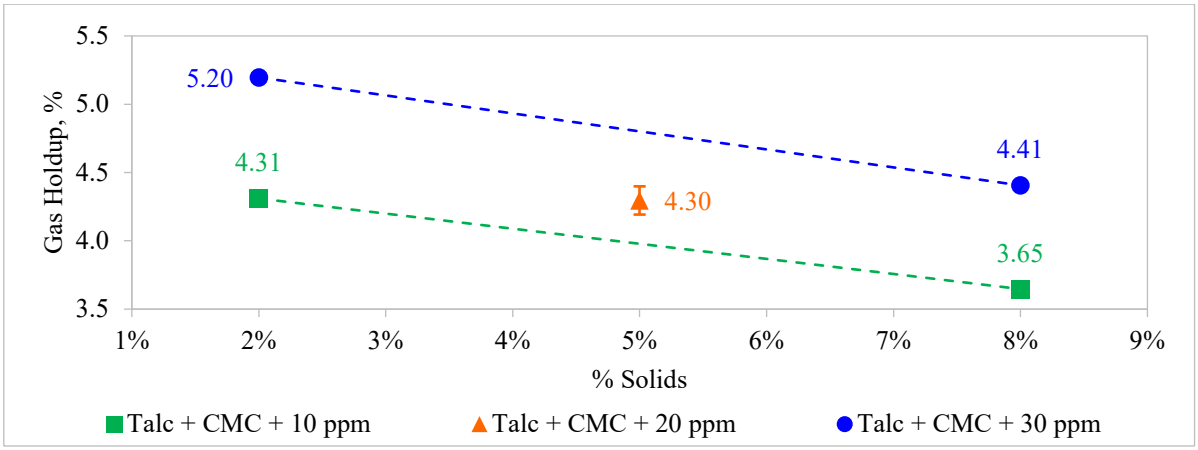

(b) Talc and CMC with 2.5 mm Sparger

Figure 16: Gas Holdups of Hydrophobic System (a) Dolomite, and (b) Talc and CMC, in a 2.5-mm Sparger Column Flotation Cell

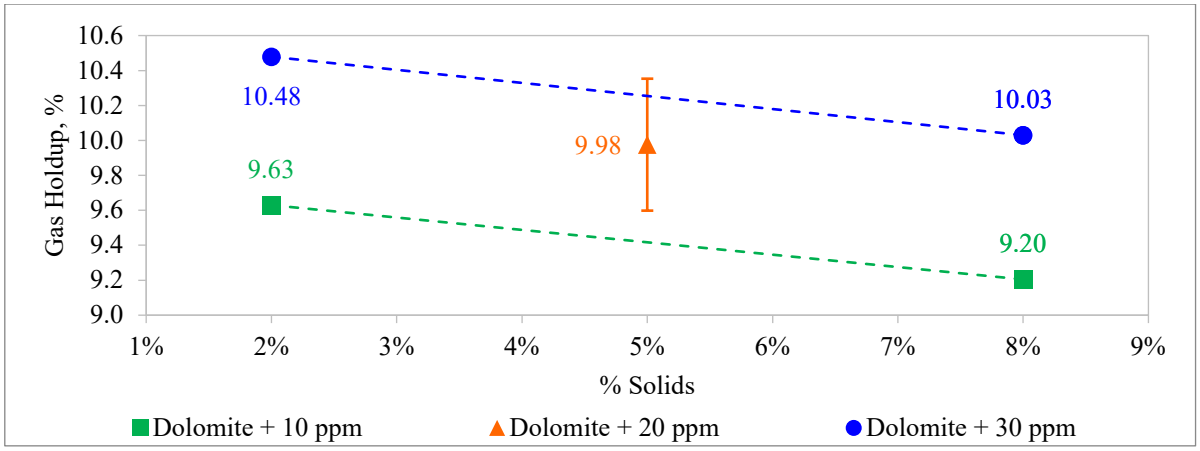

(a) Dolomite with 5.0 mm Sparger`

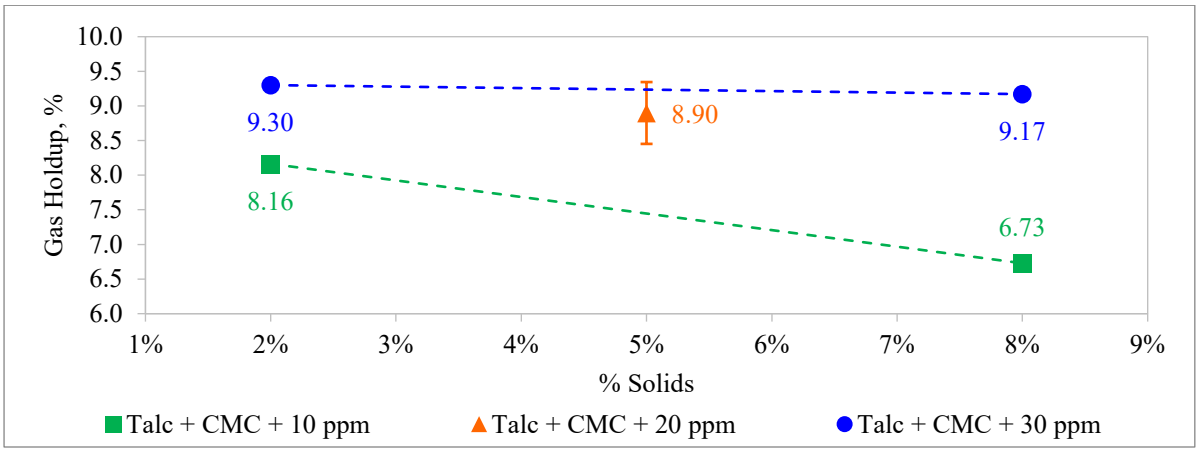

(b) Talc and CMC with 5.0 mm Sparger

Figure 17: Gas Holdups of Hydrophobic System (a) Dolomite, and (b) Talc and CMC, in a 5.0-mm Sparger Column Flotation Cell

Results of gas holdup for hydrophobic systems are displayed in Figure 14 and Figure 15 for the 2.5 and 5.0-mm spargers, respectively. Unlike the hydrophilic tests, a positive correlation between gas holdup, solid content, and frother concentration is observed in all tests. For the relationship between solid content and gas holdup, specifically, the majority of results reported in literature found an inverse correlation between the two parameters [6, 36, 37, 38, 39]. However, the opposite findings here for the positively correlated phenomena between gas holdup and solid content in the hydrophobic system could be due to the characteristics of hydrophobic particles and their interactions with bubbles. Upon bubble-particle collision, attachment is likely. Instead of bubble coalescence as seems to be the case of hydrophilic tests, the increasing solid content (or increased viscosity) prevented formation of larger bubble inhibiting the generation of higher buoyancy force [40]. As bubbles rise and collect more hydrophobic solids, they become heavier and rise at a slower rate, increasing gas holdup as a result. For talc, specifically, with its rough surface and highly hydrophobic characteristics, particle interaction with bubble could also indicate the fast wetting-film drainage dynamics and three-phase contact formation due to short area of wetting film on the rough surface particularly aided by entrapped air in tiny channels on the rough surface that bridge bubbles and talc particles [41].

For the other two tests of dolomite made hydrophobic with DDA and OA, the positive correlation strongly indicates gas holdup increases because hydrophobicity increased thereby increasing the conditions for attachment [42]. Clearly, in the case of talc, hydrophobicity may be realized without presence of frother or surfactant; but, for dolomite, DDA or OA are needed thereby causing increased bubble-particle attachment [43]. In addition, increased hydrophobicity could be aided by a rough surface (see dendrites on dolomite surface in Figure 7) which can aid film drainage, entrapped air, or both, to allow attachment. Furthermore, it could also be observed that dolomite mixing with DDA and OA showed higher

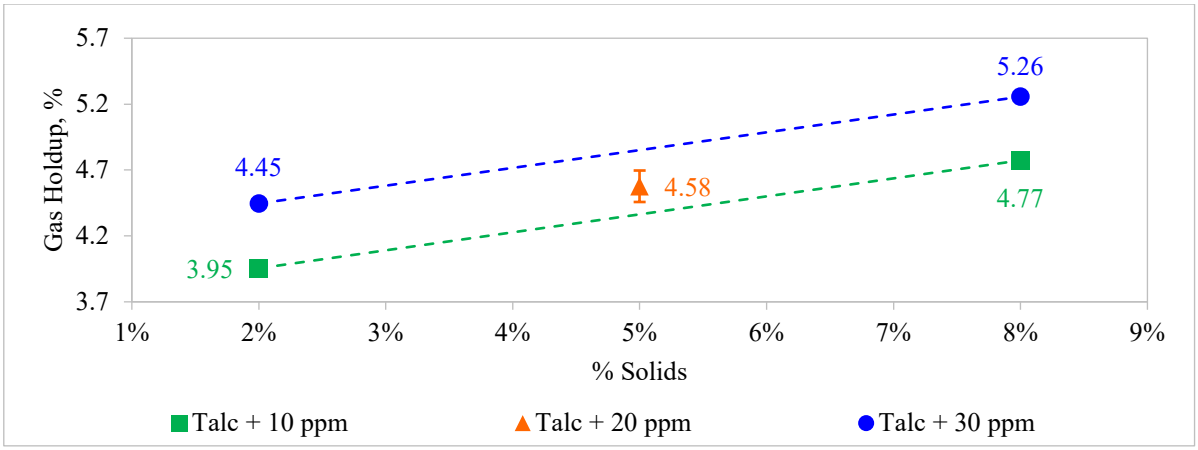

(a) Talc with 2.5 mm Sparger

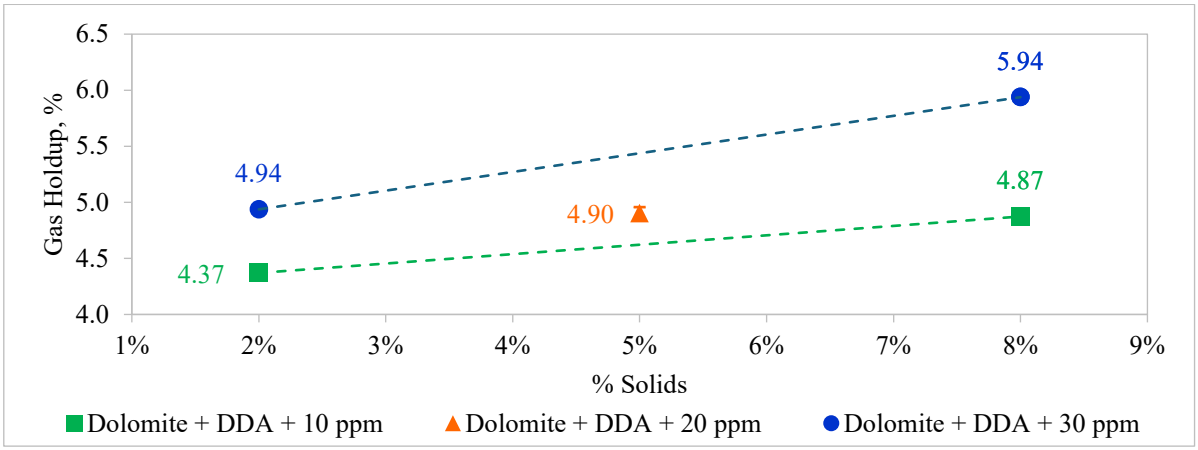

(b) Dolomite and Talc with 2.5 mm Sparger

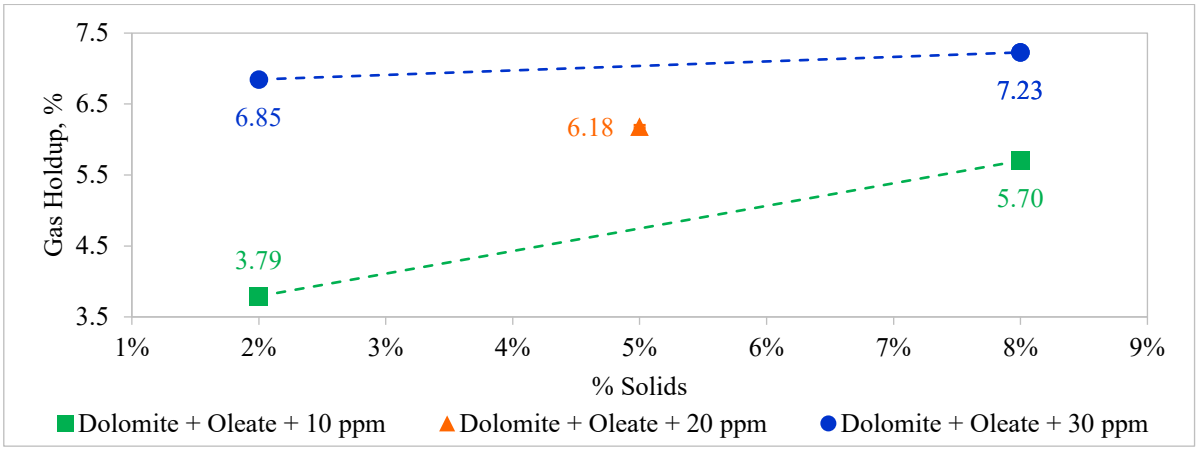

(c) Dolomite and Oleate with 2.5 mm Sparger

Figure 18: Gas Holdups of Hydrophobic System (a) Talc, (b) Dolomite and DDA, and (c) Dolomite and Oleate, in a 2.5-mm Sparger Column Flotation Cell

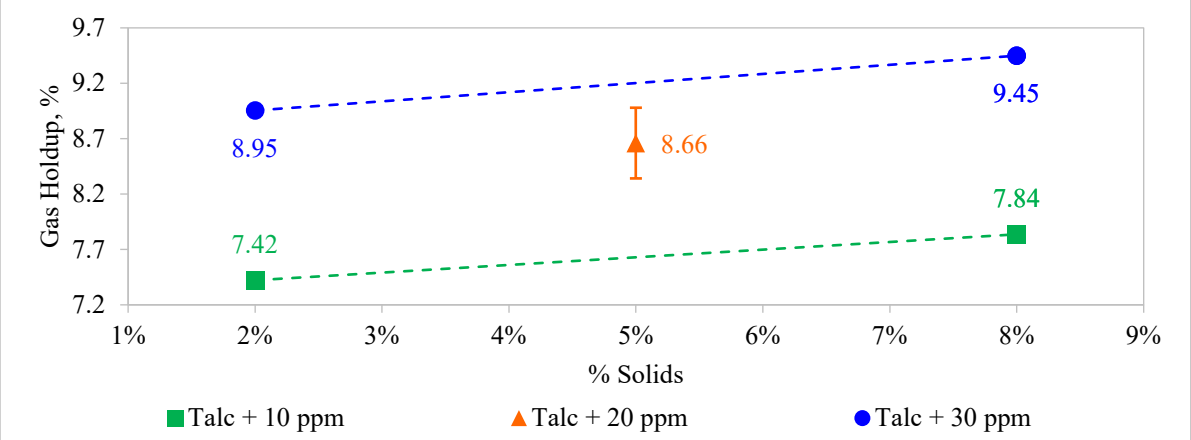

(a) Talc with 5.0 mm Sparger

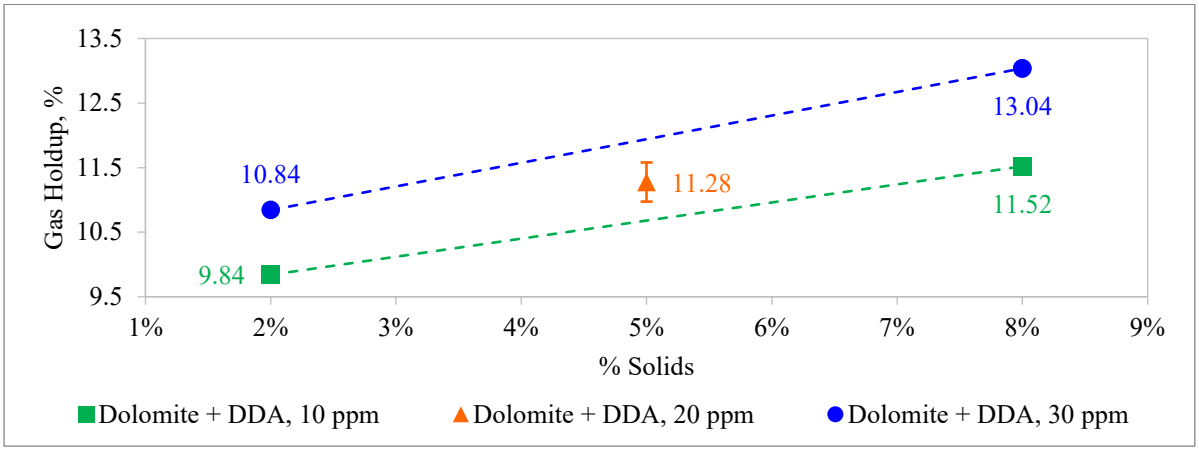

(b) Dolomite and DDA with 5.0 mm Sparger

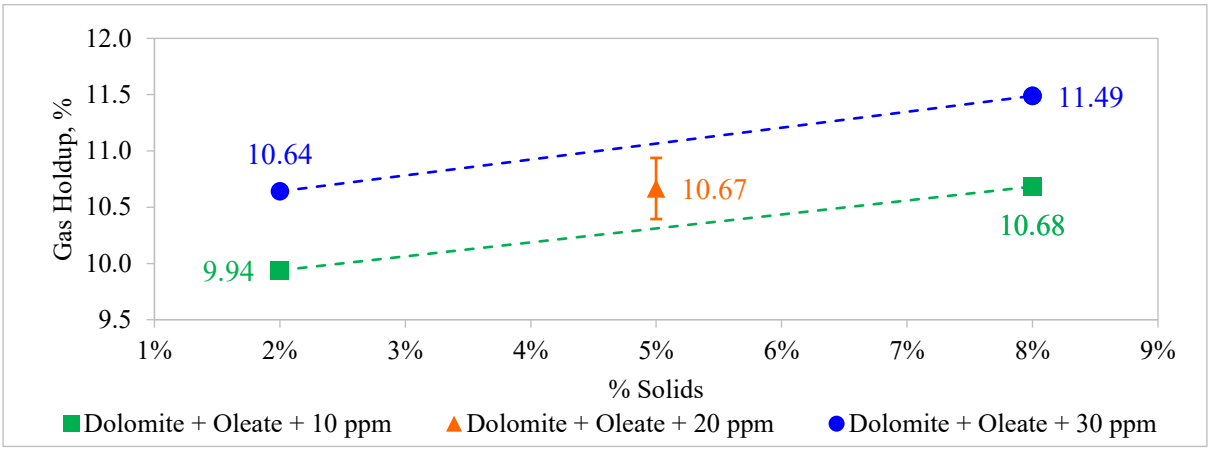

(c) Dolomite and Oleate with 5.0 mm Sparger

Figure 19: Gas Holdups of Hydrophobic System (a) Talc, (b) Dolomite and DDA, and (c) Dolomite and Oleate, in a 5.0-mm Sparger Column Flotation Cell

values of gas holdups because DDA possesses the ability to stabilize frother while OA has frothing characteristics [44, 45].

The reverse outcomes in gas holdup of dolomite in hydrophobic system and talc in hydrophilic system reflected surface characteristics alterations attributed by collector and depressant. In addition, the gas holdup data of the midpoint tests of all cases were in the realm low-low, low-high, high-low and high-high test results, indicating positive relationship between gas holdup, solid content and frother concentration for hydrophobic solids and vice versa for hydrophilic solids.

Bubble Diameters

In three-phase tests, identifying bubbles visually is difficult due to the solid color of the slurry and low contrast of lights at any angles (e.g., milky white for talc and dolomite or metallic grey for pyrite). Due to this, it is even more problematic to determine the boundary of the bubble and directly measure bubble diameter. However, bubble diameter can be calculated indirectly through various methodologies. This thesis explored two methods: Sauter mean diameter and Drift Flux Analysis (DFA); and only the reasonable method is used.

Sauter mean diameter: Sauter mean diameter considers the use of superficial gas velocity and bubble surface area flux [12]. The superficial gas velocity refers to the rise velocity of bubbles relative to cross-sectional area of the column cell, whereas bubble surface area flux refers to a total area of bubble rising per cross-sectional area per unit time which can be retrieved by using an overall rate constant. To identify this rate constant, the recovery in the froth zone as well as the bubble-particle collision efficiency must be known. The recovery in the froth zone only represents bubble compacted in the froth zone and not all bubbles in the overall column cell which are distributed across the froth and pulp zones and their interface, making some data non-representativeness [46]. Unfortunately, the scope of the test work in this thesis was conducted in closed system continuously, solids recovery was not measured, even though it could be considered 100% for hydrophobic system and 0% for hydrophilic systems because the solids were practically pure. As a result, the overall rate constant, froth zone recovery, and bubble-particle collision efficiency were undeterminable. Therefore, Sauter mean diameter was not calculated in this thesis.

Drift Flux Analysis: A method of interfacial area of bubbles examines the bubble size distribution represented by gas holdup and bubble surface area flux [12, 46]. This concept allows flexible investigation at any two points in the flotation column starting from the lowest

distance of 5.0-cm interval between the two ERT probes to as high as the interface, thereby, yielding a high degree of representative data with more accuracy. Upon gas holdup is obtained through the ERT measurement, the bubble surface area flux is calculated using simplified drift flux analysis to determine the average bubble size. The key parameters compose of slip velocity, single bubble's terminal rise velocity, and the flotation parameter as a function of Reynold's number. The slip velocity refers to the difference in velocity between air and liquid; whereas, the terminal velocity of solids settling down through the liquid. Reynold's number represents flow regime. Because the bubble diameter and Reynold's number are variable of each other's equation, the calculation is initiated by giving an initial guess of bubble diameter followed by calculating a Reynold's number. An iterative process is then used to calculate bubble diameter and another Reynold's number until the determined bubble diameter is constant, upon convergence. It is important to note that the mathematical expression shows there is an inverse relationship between gas holdup and bubble diameter (bubble diameter decreased with increasing gas holdup); hence, the concept of drift flux analysis is selected to approximate bubble diameters in this thesis.

Bubble diameter calculation tool and validation: A bubble diameter calculation tool (AminPro Add-in) was developed by a company (AminPro) using drift flux analysis principle to resolve the interfacial area of bubbles [47]. This tool was employed to calculate bubble diameters of each test (see the results in Table 4). To validate the accuracy of this tool, a high-speed camera (Photron SA-Z 2100K) obtained from Mechanical Engineering Department was also used to capture photographs of bubbles. Only snapshots of two-phase tests were taken due to difficulties to see bubbles during three-phase tests caused by mineral fines yielding an opaque slurry even at 2% solids. Also, because of froth effects, the image of bubbles in presence of frother at 10 and 30 ppm were also opaque and unclear to see bubble boundaries. Therefore, only the image of bubbles of two-phase test without frother addition (0 ppm) was used to

compare against the bubble diameter calculated by AminPro Add-in. Upon obtaining images of bubbles, this thesis used ASTM E112-13(2021) Standard Test Methods for Determining Average Grain Size to manually measure particle size of bubbles (Appendix A). In addition, 102 randomly selected bubbles were also measured (see Appendix B). The snapshots of bubbles with and without frother additions were showed in Figure 16.

Table 4: Bubble Diameter Results Calculated by DFA

Test #	Frother Concentration	Plane 1 Gas Holdup	Plane 2 Gas Holdup	Mean Gas Holdup	Plane 1 Bubble Diameter	Plane 2 Bubble Diameter	Mean Bubble Diameter
	ppm	%	%	%	mm	mm	mm
1	10	8.04	9.94	8.99	0.83	0.69	0.75
2	30	9.56	10.80	10.18	0.72	0.65	0.68
3	0	3.52	4.20	3.86	1.87	1.54	1.69

By averaging the bubble diameters that were manually measured based on ASTM and from the 102 randomly selected bubbles, the mean bubble diameter is 1.63 mm with the maximum diameter of 3.73 mm and minimum diameter of 0.93 mm. Comparing the average bubble size of 1.63 mm against the calculated bubble size by AminPro Add-in Test #3 (1.69 mm) in Table 4, both bubble diameter were similar, displaying sufficient accuracy of the calculation tool.

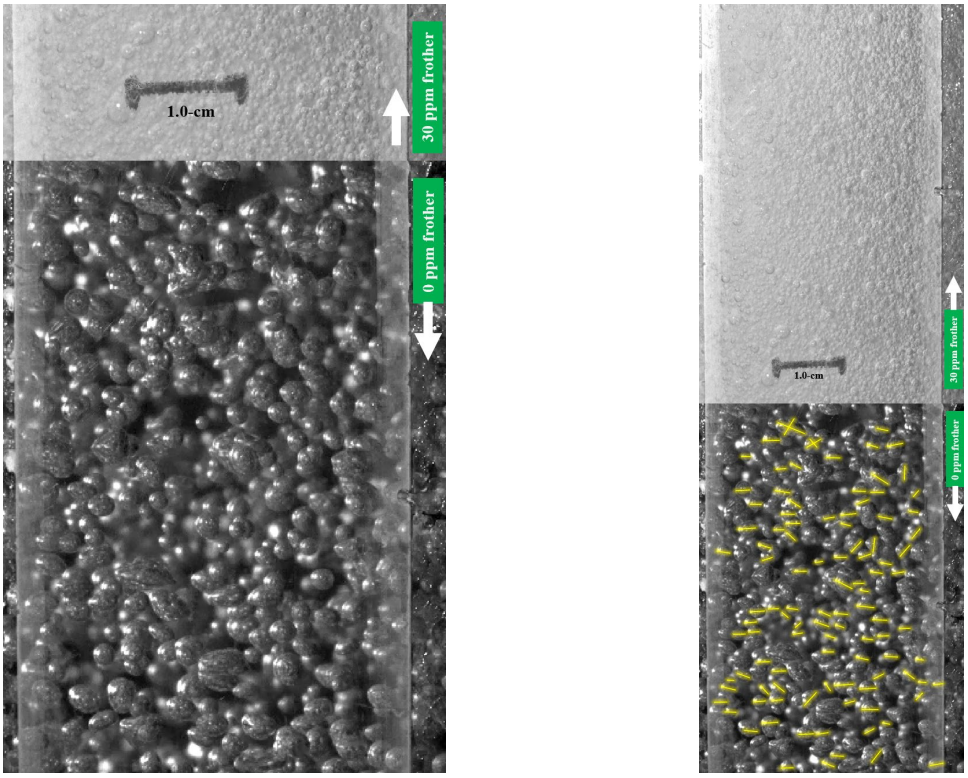

(a) Overview of bubbles with and without frother addition (b) 102 randomly selected bubbles

Figure 20: Snapshots of Bubble Diameter using High-speed Camera (a) Overviews of Bubble with and without Frother Addition, and (b) Marks of Randomly Selected Bubbles

Bubble diameter results are displayed in Figure 17. Midpoint test results of each hydrophilic and hydrophobic test were averaged into a single data set represented on the third figure from the top down.

With the same vertical scale, it was obvious to see for 2.5-mm sparger that bubble diameters at Plane 1 were consistently larger than Plane 2. While this trend was also observed for the case of 5.0-mm sparger, the bubble diameters at Plane 1 were only slightly larger than Plane 2, pointing out the rate of dispersion to be higher when the bigger sparger was used. Reasons for the larger bubble diameter in Plane 1 could be due to the geometry of Plane 1 being closer to the sparger. As air exited the sparger, a bubble formation occurred which involved air expanding from 70 psi to the pressure at the depth of the sparger; however, these bubbles were not yet completely formed undergoing a transition from turbulence to quiescent. The shear

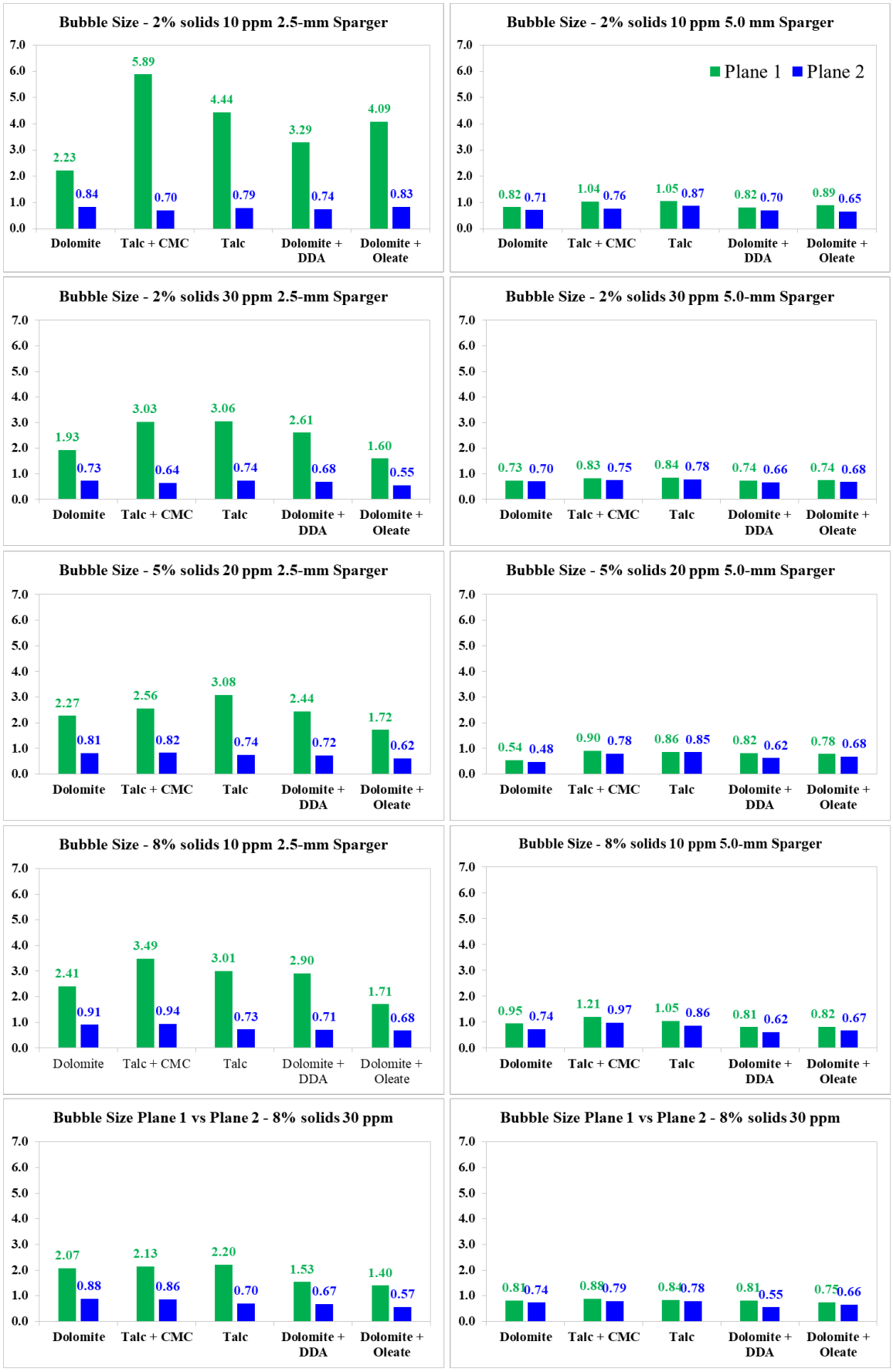

Figure 21: Bubble Diameter Results in mm of 2.5-mm (left) and 5.0-mm (right) Spargers

force between the air and sparger wall as well as the pressure difference between inside and outside of the sparger determined the size of the initially formed bubble that inherited turbulence behaviour (churn-turbulent flow regime) due to high ratio of superficial velocity to gas holdup at the area near the sparger. Large bubbles then broke down to smaller size as they reached the fully dispersed point where a steady state of axial flow started and maintained. With presence of frother, full dispersion was enhanced and achievable by Plane 2 for both hydrophilic and hydrophobic systems. As bubbles and solids collide, the bubble diameter above this point should at least remain the same or slightly increased (for hydrophobic solids due to likelihood of collision and attachment) or decreased (for hydrophilic solids due to likelihood of collision and detachment/coalescence) for the rest of the pulp zone. While it appeared that bubble diameters associated with talc were higher than dolomite, the same trend was also found for the cases of talc and dolomite mixing with reagents respectively. Reasons behind this could be due to the difference in solids density between the two solids. Additionally, the trends showed bubble diameter to decrease with frother concentration.

Table 5: Sparger Bubble Diameter Results at Plane 1 and Plane 2 (2.5-mm)

	Plane 1			Plane 2			Plane 1	Plane 2
	10 ppm			30 ppm			20 ppm	
	0% solids	2% solids	8% solids	0% solids	2% solids	8% solids	5% solids	
Hydrophilic:								
Dolomite	1.35	2.23	2.41	0.74	0.84	0.91	2.27	0.81
Talc + CMC	1.35	5.89	3.49	0.74	0.70	0.94	2.56	0.82
Hydrophobic:								
Talc	1.35	4.44	3.01	0.74	0.79	0.73	3.08	0.74
Dolomite + DDA	1.35	3.29	2.90	0.74	0.74	0.71	2.44	0.72
Dolomite + Oleate	1.35	4.09	1.71	0.74	0.83	0.68	1.72	0.62

Table 6: Bubble Diameter Results in mm at Plane 1 and Plane 2 with increasing Solids Content (5.0-mm)

	Plane 1			Plane 2			Plane 1	Plane 2
	10 ppm			30 ppm			20 ppm	
	0% solids	2% solids	8% solids	0% solids	2% solids	8% solids	5% solids	
Hydrophilic:								
Dolomite	0.94	0.82	0.95	0.68	0.71	0.74	0.54	0.48
Talc + CMC	0.94	1.04	1.21	0.68	0.76	0.97	0.90	0.78
Hydrophobic:								
Talc	0.94	1.05	1.05	0.68	0.87	0.86	0.86	0.85
Dolomite + DDA	0.94	0.82	0.81	0.68	0.70	0.62	0.82	0.62
Dolomite + Oleate	0.94	0.89	0.82	0.68	0.65	0.67	0.78	0.68

Table 5 and Table 6 tabulated bubble diameters of all tests with various colours to signify the increase or decrease trend of bubble size as solids content increased from 2 to 8%. Green cells refer to a decrease in bubble diameter. Yellow cells refer an increase in bubble diameter by 5 % of bubble size. Red cells refer to an increase in bubble diameter by more than 10% of bubble size. Data from midpoint tests displayed in the last two columns of both tables were not compared to 2 and 8% due to their froth concentrations and % solids being different.

The results of bubble diameters of non-solid tests (0% solids) were also tabulated on both tables. Bubble diameters of non-solid tests were mostly smaller than bubble diameters of

hydrophilic tests at both planes for both spargers, pointing coalescence of bubbles in presence of hydrophilic solids. On the other hand, they are mostly larger or similar bubble sizes of hydrophobic tests except for the case of Plane 1 of 2.5-mm sparger implying attachment of bubble and particles in presence of hydrophobic solids. However, the non-solid test bubble size being smaller than the hydrophobic test bubble sizes at Plane 1 of 2.5-mm sparger could be because of the effects of viscosity and different rheology due to presence of fine solids, increased solids content and increased frother.

While bubble diameter decreased with solid content for hydrophobic tests in 2.5-mm sparger column, it was mostly the case in the 5.0-mm. The tests using talc and dolomite mixing with OA were observed to have almost the same and slightly higher bubble diameters respectively. On the other side, bubble diameter at Planes 1 and 2 using both spargers were shown to increase with solids content for hydrophilic system except for the case or talc mixing with CMC where bubble diameter dropped from Plane 1 to Plane 2 by 40% (5.89 to 3.49 mm). The positively and negatively correlated relationships between bubble and solid content displayed by the tested hydrophobic and hydrophilic systems highly emphasized the phenomena of bubble-particle attachment upon collision and low chance of coalescence in the presence of true hydrophobic sample and high chance of coalescence in the presence of hydrophilic solids.

By incorporating the Young-Laplace equation which expresses positive corelation between bubble size and surface tension, bubble size should increase in presence of CMC and decrease in presence of DDA and OA. While the case of CMC in this thesis reflected findings in literature [52] as well as the principle of Laplace, it can also be caused by bubble coalescence due to presence of solids. On the other hand, the impact of DDA on bubble surface tension was reported to be peculiar [53]. This thesis observed such trend vaguely at Plane 2 while increasing bubble size was observed at Plane 1. For OA, the surface tension of bubble increased with OA

concentrations in two-phase tests [54]. However, the experiment showed an inverse relationship likely due to presence solids.

Conclusions

This thesis provided a review on column flotation modeling. While phenomenological modeling has been conducted on mechanically mixed flotation, modeling on column flotation was only empirically based. Research in this thesis also examined column flotation phenomenologically by using ERT to obtain real time two-dimensional responses of gas holdup inside the flotation column at various heights. A two-factor factorial design was used to develop experimentation for both hydrophilic and hydrophobic solids using naturally hydrophilic dolomite and naturally hydrophobic talc, respectively. To see the impacts of surface chemistry, depressant CMC was employed to turn talc into hydrophilic solids, whereas DDA and OA collectors were used to turn dolomite into hydrophobic solids. Gas holdup was used to calculate gas dispersion and bubble diameter. These three parameters were analyzed against solids content and frother concentration as a function of sparger size. The key findings which will serve to measure the metallurgical performance of column flotation for phenomenological modeling included:

- Gas holdup decreased with hydrophilic solids and was attributed to bubbles coalescence at their surfaces.
- Gas holdup increased with hydrophobic solids and was attributed to the bubbles and particles becoming attached, so they rose slower.
- Gas holdup of both solids increased with increasing frother concentrations.
- A fully dispersed axial flow was noticed at Plane 2, but the gas holdup continued to increase slightly on Plane 3 and 4 for hydrophobic tests but remained constant for hydrophilic tests. This signifies the likelihood of attachment and coalescence upon bubble-particle collision in presence of hydrophobic and hydrophilic solids, respectively.

- Bubble size had the opposite behavior of gas holdup and thereby decreased hydrophobic solids and increased with hydrophilic solids. These results confirm and emphasize there is a higher chance of bubble attachment associated with hydrophobic solids and bubble coalescence associated with hydrophilic solids.

Future Work and Recommendations

Recommendations for future work include:

- Developing a simple kinetic test (SKT)-like procedure to determine metallurgical performance (grade and recovery) of three-phase tests in column flotation;
- Appling ERT measurements to column flotation of various ores containing low amounts of valuable minerals (e.g., REE) and high amounts of valuable minerals (e.g., complex sulfides) or materials (e.g., coal);
- Examining the impact of multi-reagents with the different ores particularly collector blends; and
- Constructing compartmental phenomenological model and comparing applications to flotation columns and mechanical agitation cells;

References

[1] A. J. Lynch, G. J. Harbort, M. G. Nelson and M. G. Nelson, History of Flotation, Carlton: Australasian Institute of Mining and Metallurgy, 2010.

[2] B. A. Wills and J. A. Finch, Chapter 12 - Froth Flotation, Elsevier Ltd, 2015.

[3] S. R. Rao and J. Leja, Surface chemistry of froth flotation. Volume 1, Fundamentals, New York: Springer Science+Business Media, 2004.

[4] C. A. Hardie, G. F. Leichtle, J. A. Finch and C. O. Gomez, "Application of mineral processing techniques to the recycling of wastepaper," in Proceedings of the 30th Annual Meeting of the Canadian Mineral Processors Conference, Ottawa, 1998.

[5] J. Saththasivam, K. Loganathan and S. Sarp, "An overview of oil–water separation using gas flotation systems," Chemosphere, vol. 144, pp. 671-680, 2016.

[6] J. A. Finch and G. S. Dobby, Column Flotation, Ann Arbor: Pergamon, 1990.

[7] K. S. Moon and L. L. Siroi, "THEORY AND APPLICATION OF COLUMN FLOTATION," Canadian Government Publishing Centre, Ottawa, 1989.

[8] G. Harbort and D. Clarke, "Fluctuations in the popularity and usage of flotation," Minerals Engineering, vol. 100, pp. 17-20, 2017.

[9] J. Bouchard, A. Desbiens, R. d. Villar and E. Nunez, "Column flotation simulation and control: An overview," Minerals Engineering, vol. 22, no. 6, pp. 519-529, 2009.

[10] O. N. Manjrekar and M. P. Dudukovic, "Identification of flow regime in a bubble column reactor with a combination of optical probe data and machine learning technique," Chemical Engineering Science: X, vol. 2, 2019.

[11] P. Amelunxen and R. LaDouceur, "Applied Flotation Modelling," in SME Mineral Processing and Extractive Metallurgy Handbook, New York, 2019.

[12] L. Richard, "HIGH FIDELITY KINETIC MODEL FOR FLOTATION: APPLICATIONS TO RARE EARTH ELEMENTS AND COPPER/MOLYBDENUM SEPARATIONS," Montana Tech, Butte, 2018.

[13] R. Benson, R. Glaccum and M. Noel, "Geophysical Techniques for Sensing Buried Waste and Waste Migration," Prepared for U.S. Environmental Protection Agency, Vols. EPA-600/7-84-064, p. 256, June 1984.

[14] L. Pakzad, F. Ein-Mozaffari and P. Chan, “Using electrical resistance tomography and computational fluid dynamics modeling to study the formation of cavern in the mixing of pseudoplastic fluids possessing yield stress,” Chemical Engineering Science, vol. 63, no. 9, pp. 2508-2522, 2008.

[15] P. Holdsworth, R. LaDouceur and C. Young, “Effect of frother strength on gas dispersion in a cavitation sparger measured by electrical resistance tomography,” Elsivier, vol. 160, 2021.

[16] B. Vadlakonda and N. Mangadoddy, “Hydrodynamic study of two phase flow of column flotation using electrical resistance tomography and pressure probe techniques,” Separation and Purification Technology, vol. 184, pp. 168-187, 2017.

[17] A. Nissinen, A. Lehikoinen, M. Mononen, S. Lähteenmäki and M. Vauhkonen, “Estimation of the bubble size and bubble loading in a flotation froth using electrical resistance tomography,” Minerals Engineering, vol. 69, pp. 1-12, 2014.

[18] M. Maldonado, A. Pinto, L. Magne, C. Gomez and J. Finch, “Gas holdup estimation using Maxwell equation in flotation systems: Revisited,” Minerals Engineering, vol. 98, pp. 9-13, 2016.

[19] E. Burdukova, G. V. Leerdam, F. Prins, R. Smeink, D. Bradshaw and J. Laskowski, “Effect of calcium ions on the adsorption of CMC onto the basal planes of New York talc – A ToF-SIMS study,” Minerals Engineering, vol. 21, p. 1020–1025, 2008.

[20] C. Liu, W. Zhang, S. Song and H. Li, “A novel method to improve carboxymethyl cellulose performance in the flotation of talc,” Minerals Engineering, vol. 131, pp. 23-27, 2019.

[21] A. Semmeq, Y. Foucaud, N. E. Yamami, A. Michailovski, S. Lebègue and M. Badawi, “Hydration of magnesite and dolomite minerals: new insights from ab initio molecular dynamics,” Colloids and Surfaces A: Physicochemical and Engineering Aspects, vol. 631, 2021.

[22] J. Kou, D. Tao and G. Xu, “A study of adsorption of dodecylamine on quartz surface using quartz crystal microbalance with dissipation,” Colloids and Surfaces A: Physicochemical and Engineering Aspects, vol. 368, no. 1-3, pp. 75-83, 2010.

[23] P. Dhar, M. Thornhill and H. R. Kota, “An Overview of Calcite Recovery by Flotation,” Materials Circular Economy, vol. 2, no. 9, 2020.

[24] X. Wang and Q. Zhang, “Insight into the Influence of Surface Roughness on the Wettability of Apatite and Dolomite,” Minerals, vol. 10, no. 2, p. 114, 2020.

[25] M. Merlini, W. A. Crichton, M. Hanfland, M. Gemmi, H. Müller, I. Kupenkol and L. Dubrovinsky, “Structures of dolomite at ultrahigh pressure and their influence on the deep carbon cycle,” Proc Natl Acad Sci U S A , vol. 109, no. 34, pp. 13509-13514, 2012.

[26] ThermoFisher, “Carboxymethylcellulose sodium salt, Thermo Scientific Chemicals,” ThermoFisher Scientific, [Online]. Available: https://www.thermofisher.com/order/catalog/product/A18105.36. [Accessed 22 4 2024].

[27] ThermoFisher, “Dodecylamine hydrochloride, 99%, Thermo Scientific Chemicals,” ThermoFisher Scientific, [Online]. Available: https://www.thermofisher.com/order/catalog/product/409250100. [Accessed 22 3 2024].

[28] Sapphire, “Oleic Acid (sodium salt),” Sapphire , [Online]. Available: https://www.sapphire-usa.com/product/NS0000309460/oleic-acid-%28sodium-salt%29. [Accessed 2024 4 22].

[29] J. A. Bazar, M. Rahimi, S. Fathinia, M. Jafari, V. Chipakwe and S. C. Chelgani, Talc Flotation—An Overview, Minerals, 2021.

[30] M. O'Donoghue, The Encyclopedia of Minerals and Gemstones, London: Orbis Publishing Ltd, 1990.

[31] R. Marouf, K. Marouf-Khelifa, J. Schott and A. Khelifa, “Zeta potential study of thermally treated dolomite samples in electrolyte solutions,” Microporous and Mesoporous Materials, 2009.

[32] O. S. Pokrovsky, J. Schott and F. Thomas, “Dolomite surface speciation and reactivity in aquatic systems,” Geochimica et Cosmochimica Acta, 1999.

[33] I. Mohammed, D. A. Shehri, M. Mahmoud, M. S. Kamal, M. Arif, O. S. Alade and S. Patil, “Investigation of Surface Charge at the Mineral/Brine Interface: Implications for Wettability Alteration,” Colloidal Materials and Interfaces, vol. 9, 2022.

[34] M. H. Derkani, A. J. Fletcher, M. Fedorov, W. Abdallah, B. Sauerer, J. Anderson and Z. J. Zhang, “Mechanisms of Surface Charge Modification of Carbonates in Aqueous Electrolyte Solutions,” Colloids and Interfaces, vol. 3, no. 4, 2019.

[35] A. Nguyen and H. J. Schulze, Colloidal Science of Flotation, Boca Raton: CRC Press, 2003.

[36] G. Hanly, D. Fornasiero, J. Ralston and R. Sedev, “Electrostatics and Metal Oxide Wettability,” The Journal of Physical Chemistry, vol. 115, no. 30, p. 14914–14921, 2011.

[37] A. Niecikowska, M. Krasowska, J. Ralston and K. Malysa, “Role of Surface Charge and Hydrophobicity in the Three-Phase Contact Formation and Wetting Film Stability under Dynamic Conditions,” The Journal of Physical Chemistry, vol. 116, no. 4, p. 3071–3078, 2012.

[38] D. Pashkevich, R. Li, O. Kökkılıç and K. E. Waters, “Investigations of Monomineralic Flotation of Galena, Sphalerite, and Pyrite at Different Temperatures,” Minerals, vol. 13, no. 5, 2023.

[39] C. Liu, W. Zhang, S. Song and a. H. Li, “A novel method to improve carboxymethyl cellulose performance in the flotation of talc,” Minerals Engineering, vol. 131, pp. 23-27, 2019.

[40] S. Banisi, J. Finch, A. Laplante and M. Weber, “Effect of solid particles on gas holdup in flotation columns—I. Measurement,” Chemical Engineering Science, vol. 50, no. 14, pp. 2329-2334, 1995.

[41] S. H. Kuan, “The Effect of Solids on Gas Holdup, Bubble Size and Water Overflow Rate in Flotation,” Department of Mining, Metals and Materials Engineering, McGill University , Montreal, 2009.

[42] B. S and F. J. A., “Technical Note: Reconciliation of Bubble Size Estimation,” Minerals Engineering, vol. 7, no. 12, p. 1555–1559, 1994.

[43] S. Kara, B. G. Kelkar, Y. T. Shah and N. L. Carr, “Hydrodynamics and axial mixing in a three-phase bubble column,” Industrial Engineering Chemistry Process Design and Development, vol. 21, no. 4, pp. 584-594, 1982.

[44] R. Escudero and R. E. Pérez, “Viscosity and Drift Flux Analysis in a Two Phase System,” International Journal of Advances in Engineering and Management, vol. 3, no. 12, pp. 623-630, 2021.

[45] M. Li, Y. Xing, C. Zhu, Q. Liu, Z. Yang, R. Zhang, Y. Zhang, Y. Xia and a. X. Gui, “Effect of roughness on wettability and floatability: Based on wetting film drainage between bubbles and solid surfaces,” International Journal of Mining Science and Technology, vol. 32, no. 6, pp. 1389-1396, 2022.

[46] S. M. Bulatovic, 1 - Classification of Flotation Reagents, Petersborough: Elsevier, 2007, pp. 1 - 3.

[47] N. Churaev, “On the forces of hydrophobic attraction in wetting films of aqueous solutions,” Colloids and Surfaces A: Physicochemical and Engineering Aspects, vol. 79, no. 1, pp. 25-31, 2001.

[48] A. Atrafi and M. Pawlik, “Foamability of fatty acid solutions and surfactant transfer between foam and solution phases,” Minerals Engineering, vol. 100, pp. 99-108, 2017.

[49] X. Luo, Q. Lin, S. Wen, Y. Wang, H. L. 1, L. Q. 1, X. W. 1, Y. Z. 1 and Z. Song, “Effect of Sodium Dodecyl Sulfonate on the Foam Stability and Adsorption Configuration of Dodecylamine at the Gas-Liquid Interface,” National Center for Biotechnology Information, vol. 37, no. 3, pp. 1235-1246, 2021.

[50] A. Vazirizadeh, J. Bouchard and R. d. Villar, “On the relationship between hydrodynamic characteristics and the kinetics of column flotation. Part I: Modeling the gas dispersion,” Minerals Engineering, vol. 74, pp. 207-215, 2015.

[51] P. Amenluxen and C. Young, “AminPro Add-in for Microshoft Excel,” AminPro.

[52] Z. Zhang, L. Ou, S. Jin and H. Zhou, “The effect of sodium carboxymethyl cellulose on the entrainment of zoisite in flotation,” Physicochemical Problems of Mineral Processing, vol. 57, no. 2, pp. 34-48, 2020.

Appendices

Appendix A: ASTM Standard Test Methods for Determining Average Grain Size

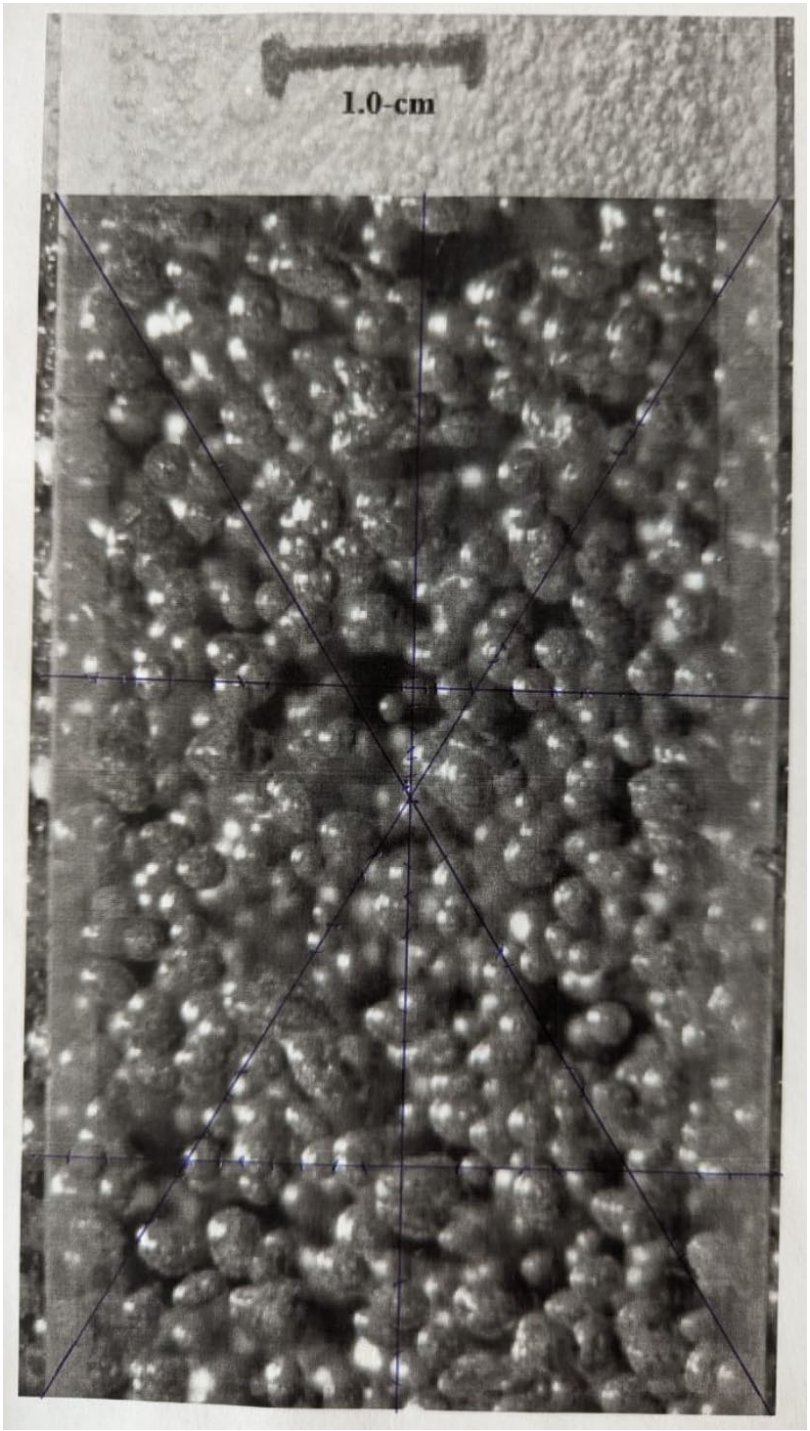

1-cm length		3.3
#	Bubble Length	cm
1	0.45	1.36
2	0.50	1.52
3	0.30	0.91
4	0.65	1.97
5	0.30	0.91
6	0.40	1.21
7	0.30	0.91
8	0.40	1.21
9	0.40	1.21
10	0.40	1.21
11	0.35	1.06
12	0.35	1.06
13	0.50	1.52
14	0.45	1.36
15	0.55	1.67
16	0.50	1.52
17	0.40	1.21
18	0.30	0.91
19	0.40	1.21
20	0.60	1.82
21	0.40	1.21
22	0.45	1.36
23	0.40	1.21
24	0.60	1.82
25	0.70	2.12
26	0.50	1.52
27	0.60	1.82
28	0.45	1.36
29	0.60	1.82
30	0.60	1.82
31	0.55	1.67
32	0.55	1.67
33	0.45	1.36
34	0.55	1.67
35	0.55	1.67
36	0.50	1.52
37	0.45	1.36
38	0.75	2.27
39	0.50	1.52
40	0.50	1.52
41	0.35	1.06
42	0.50	1.52
43	0.45	1.36
44	0.25	0.76
45	0.30	0.91
46	0.45	1.36
47	0.65	1.97
48	0.35	1.06
49	0.75	2.27
50	0.45	1.36

Appendix B: 102 spots of randomly selected bubbles

Opposite	0.66
Adjacent	0.99
Hypotenous equivalent to mm	1.19

Average bubble diameter, mm	1.57
Maximum bubble diameter, mm	3.73
Minimum bubble diameter, mm	0.93

#	Op	Adj	Hyp	Convert to mm
1	0.03	0.15	0.15	1.29
2	0.06	0.19	0.20	1.67
3	0.15	0.24	0.28	2.38
4	0.15	0.12	0.19	1.61
5	0.21	0.01	0.21	1.77
6	0.05	0.17	0.18	1.49
7	0.21	0.03	0.21	1.78
8	0.17	0.15	0.23	1.91
9	0.09	0.09	0.13	1.07
10	0.02	0.14	0.14	1.19
11	0.01	0.2	0.20	1.68
12	0.09	0.1	0.13	1.13
13	0.13	0.14	0.19	1.61
14	0.04	0.15	0.16	1.30
15	0.13	0.08	0.15	1.28
16	0.08	0.22	0.23	1.97
17	0.01	0.18	0.18	1.52
18	0.04	0.14	0.15	1.22
19	0.02	0.18	0.18	1.52
20	0.03	0.18	0.18	1.53
21	0.01	0.2	0.20	1.68
22	0.01	0.22	0.22	1.85
23	0	0.18	0.18	1.51
24	0.03	0.23	0.23	1.95
25	0.01	0.2	0.20	1.68
26	0.12	0.21	0.24	2.03
27	0	0.14	0.14	1.18
28	0	0.16	0.16	1.34
29	0.07	0.17	0.18	1.55
30	0.01	0.2	0.20	1.68
31	0.08	0.09	0.12	1.01
32	0.02	0.15	0.15	1.27
33	0.01	0.17	0.17	1.43
34	0.13	0.26	0.29	2.44
35	0.05	0.15	0.16	1.33
36	0.01	0.17	0.17	1.43
37	0.2	0.13	0.24	2.00
38	0.04	0.18	0.18	1.55
39	0	0.21	0.21	1.76
40	0	0.21	0.21	1.76
41	0	0.19	0.19	1.60
42	0.02	0.12	0.12	1.02
43	0.13	0.12	0.18	1.49
44	0.03	0.21	0.21	1.78
45	0	0.2	0.20	1.68
46	0.01	0.2	0.20	1.68
47	0.01	0.19	0.19	1.60
48	0.13	0.16	0.21	1.73
49	0.02	0.18	0.18	1.52
50	0.05	0.22	0.23	1.90
51	0.02	0.29	0.29	2.44
52	0.04	0.13	0.14	1.14
53	0.02	0.19	0.19	1.61
54	0	0.16	0.16	1.34
55	0.06	0.2	0.21	1.75
56	0	0.16	0.16	1.34
57	0.02	0.27	0.27	2.28
58	0.03	0.23	0.23	1.95
59	0.01	0.22	0.22	1.85
60	0.25	0.15	0.29	2.45
61	0.02	0.19	0.19	1.61
62	0.01	0.17	0.17	1.43
63	0.01	0.11	0.11	0.93
64	0.08	0.18	0.20	1.66
65	0.01	0.23	0.23	1.93
66	0.02	0.15	0.15	1.27
67	0.01	0.13	0.13	1.10
68	0.07	0.19	0.20	1.70
69	0.04	0.19	0.19	1.63
70	0.01	0.2	0.20	1.68
71	0.01	0.17	0.17	1.43
72	0.01	0.26	0.26	2.19
73	0.01	0.16	0.16	1.35
74	0.07	0.16	0.17	1.47
75	0.16	0.15	0.22	1.84
76	0.05	0.24	0.25	2.06
77	0.17	0.41	0.44	3.73
78	0.04	0.21	0.21	1.80
79	0.02	0.2	0.20	1.69
80	0.12	0.16	0.20	1.68
81	0.04	0.2	0.20	1.71
82	0.06	0.23	0.24	2.00
83	0.07	0.15	0.17	1.39
84	0.2	0.18	0.27	2.26
85	0.11	0.01	0.11	0.93
86	0.01	0.23	0.23	1.93
87	0.01	0.26	0.26	2.19
88	0.03	0.27	0.27	2.28
89	0.02	0.21	0.21	1.77
90	0.02	0.19	0.19	1.61
91	0.02	0.16	0.16	1.36
92	0.01	0.2	0.20	1.68
93	0.01	0.18	0.18	1.52
94	0.01	0.18	0.18	1.52
95	0	0.26	0.26	2.19
96	0.13	0.12	0.18	1.49
97	0.08	0.18	0.20	1.66
98	0.02	0.24	0.24	2.02
99	0.04	0.15	0.16	1.30
100	0.02	0.13	0.13	1.11
101	0.11	0.18	0.21	1.77
102	0.18	0.14	0.23	1.92